RSC Advances

PAPER

View Article Online
View Journal | View Issue

Cite this: *RSC Adv.*, 2026, **16**, 5515

Novel pH-responsive pectin-based hybrid smart hydrogels for in vitro drug release and in vivo wound healing applications

Hirra Manzoor, Nasima Arshad, * Muhammad A. U. R. Qureshi and Sher Qadar

Despite their exceptional biocompatibility and non-toxicity, pectin-based hydrogels suffer from poor mechanical strength, water sensitivity and high instability, which limit their utilization in the biomedical sector. Therefore, main objective behind this study was to develop integrated pectin-based hydrogel system to improve mechanical and structural properties of hydrogels for biomedical applications. Multifunctional hydrogels were formulated to integrate the gel-forming capabilities and biocompatibility of polyvinyl alcohol (PVA) and pectin, with the crosslinking and structural reinforcement of 3-aminopropyltriethoxysilane (APTES), and the antimicrobial and drug-loading capabilities of graphene oxide (GO) fillers. Using varied GO concentrations, pectin/PVA/APTES/GO hydrogel series PPG (−2.5, −5, −7.5, and −10) was synthesized, and samples' structural integrity, amorphous nature, porous morphology, and thermal stability were characterized. The hydrogels demonstrated high cell viability, biodegradation, and antibacterial activity, and their swelling in distilled water (DW) reached a maximum value of 3300% in 120 min. The greatest degree of swelling was observed at pH 8 in both buffered and non-buffered solutions. Following the Higuchi, zero-order, and Korsmeyer-Peppas models for controlled release kinetics, 91.44% of levofloxacin (LVX) was released from the drug-loaded hydrogel (DPPG) within 3.5 hours in a PBS (pH 7.4) solution. Furthermore, *in vivo* wound healing studies demonstrated excellent results, especially for the drug-loaded hydrogel DPPG, where the healing rate was 100% on day 7. The outstanding characteristics of the fabricated pectin-based hydrogels enhance their potential for antimicrobial wound dressing and controlled drug delivery applications.

Received 30th October 2025
Accepted 4th January 2026

DOI: 10.1039/d5ra08329j

rsc.li/rsc-advances

1 Introduction

Traditional drug delivery systems face challenges such as uncontrolled release, low bioavailability, and poor targeting, leading to systemic toxicity and side effects. Therefore, advanced methods are needed to improve their precision and outcomes.[1,2] Hydrogels offer a promising alternative due to their biodegradable, non-toxic, and biocompatible properties. Their responsive and adaptable structure makes them ideal for use in drug delivery and biological applications.[3,4] Hydrogels are three-dimensional, crosslinked polymeric networks composed of either synthetic or natural polymers. They can absorb and hold onto a lot of water without losing their structure. Their porous nature and the presence of hydrophilic groups allow them to swell to many times their dry weight.[5,6] Swelling in hydrogels occurs because of secondary forces, covalent bonding and chain entanglement. Hydrogel swelling occurs in three primary stages, *i.e.*, water diffusion, polymer chain relaxation and expansion. The distinctive and exceptional characteristics of hydrogels make them highly appropriate for a range of biomedical applications.[7,8] A variety of characteristics, such as their composition, origin, structure, crosslinking type, and stimulus-reactivity, may also be used to categorize them.[9,10] Stimuli-responsive hydrogels have the ability to modify their physical and chemical properties and are often referred to as "smart hydrogels".[11,12] Hydrogel synthesis involves the formation of a gel-like structure by the crosslinking of polymeric chains either by physical or chemical interactions.[13,14] The solution casting method of hydrogel synthesis is a simple, reproducible and straightforward technique.[15,16]

Natural polymers are frequently utilized in hydrogel formation due to their advantageous properties, such as low cost, easy accessibility, compatibility with biological systems, ability to degrade naturally, and environmentally friendly characteristics.[17,18] Pectin is a complex polymer consisting primarily of α-(1→4)-linked D-galacturonic acid residues.[19,20] Whether these residues are free carboxylic acid groups or esterified with methanol will define the degree of esterification (DE) of these residues.[21,22] Pectin comes from plant cell walls, usually apple pomace or citrus peels. There are various methods for extracting pectin, and each method can influence both quality and production rate. Pectin acts as a thickening agent, emulsifier,

Department of Chemistry Allama Iqbal Open University, Islamabad, Pakistan. E-mail: nasimaa2006@yahoo.com; nasima.arshad@aiou.edu.pk; hirramanzoor@gmail.com; aneesqureshi287@gmail.com; sherqadar@gmail.com

stabilizer and gelling agent.[23] The versatility of this biopolymer is associated with its biocompatibility, biodegradability, and prebiotic, gut health supporting, anti-inflammatory and antioxidant properties.[24–26] Pectin's film-forming ability makes it useful in food preservation and drug delivery systems. Its mechanical properties can be tailored for various applications through crosslinking.[27,28]

While hydrogels based on natural polymers have advantages (including sustainability and bioactivity), they often suffer from disadvantages like reduced mechanical strength and heterogeneous properties due to source variability.[29,30] Such challenges can be overcome by blending them with synthetic polymers or employing hybrid crosslinking systems.[31–33] PVA is a versatile synthetic polymer known for its water solubility, flexibility, and biodegradability under specific conditions. It provides strong mechanical stability that can be further improved by crosslinking, and shows notable resistance against chemicals, solvents, and oils.[34,35] PVA is commonly used as a stabilizer, thickener, and adhesive in various industries, including textiles, papermaking, food packaging, and biomedical applications such as contact lenses and surgical threads.[30] Its biocompatibility and eco-friendly nature make it a tempting alternative to other synthetic polymers, contributing to its use in diverse products from consumer goods to biomedical applications.[35] Fillers are substances that can be incorporated into hydrogels to enhance their thermal, mechanical, or functional characteristics.[36,37] Active fillers (*e.g.*, GO and its derivatives) confer mechanical reinforcement as well as stimuli-responsive properties on hydrogels. GO improves the elasticity, tensile strength and conductivity of hydrogels while providing hydrophilicity and bioactive properties such as antioxidant and antibacterial activities.[4,38]

LVX is a fourth-generation fluoroquinolone antibiotic with several uses as an anti-inflammatory, antibacterial, and antidysentery drug; its structural formula is shown in Fig. 1. LVX is effective against both Gram-positive and Gram-negative bacterial infections, as well as "atypical" ones.[39] It is extensively dispersed throughout the body, with an average volume of distribution of 1.1 L kg^{-1}.[29] With normal renal function, the half-life for plasma elimination is 6–8 hours. Approximately 80% of this broad range antibiotic is eliminated *via* the urinary route without having any therapeutic effect.[40]

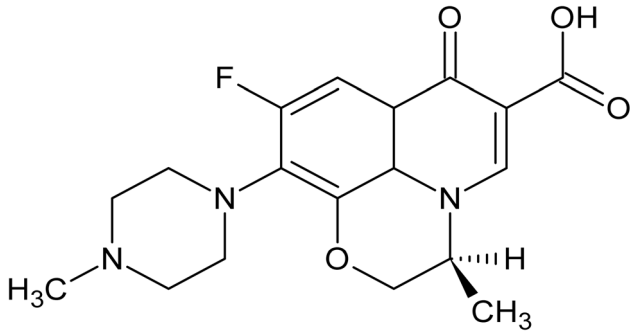

Fig. 1 The chemical structure of LVX.

In the current research, we have synthesized and characterized novel GO-reinforced pectin/PVA/APTES/GO hydrogels and investigated their pH sensitivity, biodegradability, and antibacterial and cytocompatibility efficiency. We further explored the LVX-loaded hydrogel for controlled release and wound healing properties. Pectin/PVA/APTES/GO hydrogel's novelty stems from its APTES-mediated crosslinking (replacing toxic glutaraldehyde) and GO integration, which enhance structural stability, pH responsiveness, and mechanical strength while enabling sustained LXV release *via* π–π interactions. Unlike conventional hydrogel systems, the synergy of PVA's film-forming properties and pectin's biodegradability creates a tunable, biodegradable matrix, while GO introduces greater strength and stability that was lacking in earlier reports for clay or cellulose-reinforced hydrogels.[41–43] The design addresses burst-release limitations, improves drug-loading capacity, and offers sharper pH sensitivity, positioning it as a multifunctional platform for precise, sustained antibiotic delivery in dynamic environments.

2 Experimental

2.1. Chemicals

Pectin (low methoxy content, CAS No. 9000-69-5, ≤10% moisture, galacturonic acid, ≥74.0%), PVA (CAS No. 9002-89-5), APTES (CAS No. 919-30-2, 99%), potassium chloride (CAS No. 7447-40-7), potassium dihydrogen phosphate (99%, CAS No. 9002-89-5), calcium chloride (anhydrous, CAS No. 10043-52-4), sodium hydroxide (CAS No. 1310-73-2), proteinase-K (CAS No. 39450-01-6), and graphite powder (CAS No. 7782-42-5) were purchased from Sigma-Aldrich, Germany. Nitric acid (65%, CAS No. 7697-37-2), hydrochloric acid (37%, CAS No. 7647-01-0), sulfuric acid (95–98%, CAS No. 7664-93-9), sodium chloride (CAS No. 7647-14-5) and ethylene glycol (CAS No. 107-21-1, MW: 62.07 g mol^{-1}) were obtained from Merck, Germany. Potassium permanganate (CAS No. 7722-64-7, MW: 158.03 g mol^{-1}), ethanol (CAS No. 64-17-5, MW: 46.07 g mol^{-1}) and methanol (CAS No. 67-56-1, MW: 32.04 g mol^{-1}) were bought from BDH England. Hydrogen peroxide (30%, CAS No. 7722-84-1, MW: 34.01 g mol^{-1}) and disodium hydrogen phosphate (CAS No. 7558-79-4) were purchased from Dabur, India. Glycerin (CAS No. 56-81-5), sodium azide (MW: 65.01 g mol^{-1}) and LVX drug (MW: 361.368 g mol^{-1}) were sourced from Wilson's Pharmaceuticals, Islamabad, Pakistan.

2.2. GO synthesis

GO synthesis was conducted *via* a modified Hummers' method.[44] Graphite powder (15 g) was soaked and left for 3 days in a HNO_3 and H_2SO_4 mixture (30 : 30 mL). After the addition of 200 mL of DW, the mixture was centrifuged at 6000 rpm, utilizing a Hermle Labortechnik Germany centrifuge machine, model Z 326. Black precipitates in the lower layer were heated for 3 hours at 70 °C, giving expanded graphite. Next, 4 g of expanded graphite was added to 75 mL of H_2SO_4 and stirred for 20 minutes. Then, in an ice bath, 12 g of $KMnO_4$ was added slowly with stirring for 1 hour. A brownish mixture was obtained

by adding 375 mL of deionized water after 2 hours of heating at 90 °C. Then, 2 mL of H_2O_2 was added, followed by centrifugation at 6000 rpm and alternative rinsing with DI water and 1 M HCl for purification. A thick GO suspension was obtained after 1.5 hours of heating. The GO precipitates were then dried at 60 to 70 °C, ground, and stored for future use.

2.3. Synthesis of hydrogels

The first step in the hydrogel synthesis involved dissolving 0.5 g of pectin and 0.5 g of PVA separately in 50 and 40 mL of DW. The two polymeric solutions were then combined at 70 °C and stirred for two hours. Following that, GO (2.5, 5, 7.5, and 10 mg) was sonicated for 30 minutes in 10 mL of DW. It was then added to the polymeric solution and mixed for an hour at 70 °C. Then, 20 μL APTES was mixed with 10 mL methanol and poured dropwise into the blending mixture while being constantly stirred for an additional hour. Finally, 20 μL of glycerin was introduced to improve the flexibility of the hydrogels and prevent brittleness. Hydrogels were then formed by transferring the solution into plastic Petri dishes, followed by air-drying. The hydrogels were named PPG (the control, lacking GO), PPG-2.5, PPG-5, PPG-7.5, and PPG-10, which contained 2.5, 5, 7.5, and 10 mg of GO, respectively. PPG-7.5 was loaded with 50 mg LVX and denoted as DPPG (the detailed procedure is given under the drug loading and release section). The composition of the pectin/PVA/APTES/GO hydrogels is displayed in Table 1, together with the exact ratios of each ingredient used in the formulation.

2.4. Hydrogel characterizations

A Nicolet iS10 spectrometer from Thermo Fisher Scientific (Brookhaven, USA) was used to conduct Fourier transform infrared (FTIR) spectroscopic analysis of the hydrogels to investigate the structural properties of each sample. Prior to scanning each hydrogel, it was vacuum-dried. Triangular apodization was used and spectra were obtained at a resolution of 2 cm^{-1}. Thermo-gravimetric analysis (TGA) of the prepared hydrogels was conducted using a thermal analysis (TA) instrument (model Q50, Newcastle, USA). The device had a platinum pan that held 5 mg of hydrogel material that was heated at 10 °C per minute in an inert atmosphere between 15 and 700 °C. The inert atmosphere for the analysis was achieved by continuously purging with nitrogen at a flow rate of 40 mL per minute. The synthesized hydrogels were further analyzed by X-ray diffraction (XRD) using an X'Pert Pro diffractometer, PANalytical Almelo, Netherlands. Cu Kα radiation with a wavelength of 1.544 Å was used with the scan step size of 0.025°, and the 2θ working range was 5°–80°. Scanning electron microscopy (SEM) examination was carried out using a MIRA3 TESCAN instrument, manufactured in Brno, Czech Republic. Initially, the hydrogel sample was affixed to a carbon conductive tape, followed by the application of a tungsten (W) coating at a rate of 0.8 nm per second for a duration of 92 seconds using the Safematic CCU-010 sputter coater. After that, the samples were examined at different magnifications.

Table 1 The compositions of GO-reinforced pectin/PVA/APTES/GO hydrogels

	Compositional details		
Hydrogels	Pectin (g)/PVA (g)/APTES (μL)	GO (mg)	LVX (mg)
PPG (control)	0.5/0.5/20	0	—
PPG-2.5	0.5/0.5/20	2.5	—
PPG-5	0.5/0.5/20	5	—
PPG-7.5	0.5/0.5/20	7.5	—
PPG-10	0.5/0.5/20	10	—
DPPG	0.5/0.5/20	7.5	50

2.5. *In Vitro* analyses

2.5.1. Biodegradation. Hydrogels are biodegradable, involving the breakdown of complex polymers into simpler products. This reduces their accumulation in living organisms. The biodegradation rate of hydrogels was studied in PBS (phosphate-buffered saline); proteinase-K solutions were used, and the biodegradation percentage was determined using eqn (1):

$$\text{Biodegradation } (\%) = \frac{W_o - W_t}{W_o} \times 100 \quad (1)$$

where W_o is the initial weight of the hydrogel and W_t is the weight of the hydrogel removed from PBS and proteinase-K solutions (after removing the surface water) at pre-determined intervals. Pre-weighed, sterilized, and cleaned hydrogels were immersed in 25 mL of PBS at room temperature. Weight loss was measured on days 1, 3, 7, 10, 14, and 21. For enzymatic degradation, 0.2 mg mL^{-1} proteinase-K was prepared in PBS, followed by the addition of 0.29 g $CaCl_2$. Next, 0.01% w/v NaN_3 was added as a precaution to stop the growth of microorganisms. Then, a precisely measured pre-weighed quantity of hydrogel was added to the enzymatic solution. Each sample was incubated at 37 °C, and the weight loss of dried hydrogels on days 1, 3, and 7 was compared.

2.5.2. Cell viability. The ASAB cell culture core of the National University of Sciences and Technology (NUST) provided human embryonic kidney cells (HEK-293), and an MTT assay was performed to analyze the cell viability of the hydrogel against these cells. The HEK-293 cells were grown in Dulbecco's Modified Eagle's Medium (DMEM). Here, 2 mg of hydrogel was used to seed 1×10^4 cells, which were then incubated at 37 °C. As a reference group, cells without hydrogel were used. After 48 hours, the absorbance was determined using a Bio-Rad absorbance microplate reader, model PR4100 (Washington, DC, USA). The cell viability was evaluated using eqn (2) after three cell line trials:

$$\text{Cell viability } (\%) = \frac{\text{Sample absorbance}}{\text{Reference absorbance}} \times 100 \quad (2)$$

2.5.3. Swelling. To assess each hydrogel's swelling behavior, swelling experiments were conducted. Pre-weighed amounts of dry hydrogel (10 mg) were immersed in DW.

Additionally, weight measurements of the swollen hydrogel were made at regular intervals. A tissue paper was used to remove the extra solvent in the beaker before weighing. The hydrogels' swelling capacity was also assessed in the same stream at pH levels of 2, 4, 6, 7, 8, and 10 in both buffered and non-buffered solutions. Similarly, this research explored the influence of varying concentrations (0.2, 0.4, 0.6, 0.8, and 1M) of NaCl and $CaCl_2$ solutions on the swelling characteristics of the hydrogels. Eqn (3) was used to determine each hydrogel's swelling capacity:

$$\text{Swelling } (\%) = \frac{W_s - W_d}{W_d} \times 100 \quad (3)$$

where W_s represents the weight of the swollen hydrogel and W_d represents the weight of the dried hydrogel. Using eqn (4), it is possible to explain the diffusion mechanism by which solvents or water enter and exit hydrogels.

$$F = kt^n \quad (4)$$

"F" stands for fractional swelling, "k" for the swelling rate constant, "t" for the swelling duration, and "n" for the swelling exponent. The value of "n" indicates the type of diffusion mechanism occurring as water or solvent penetrates the hydrogel network.

2.5.4. Antibacterial assay. Using the disc diffusion method, each hydrogel's antibacterial activity was tested against *Escherichia coli (E. coli)* and *Staphylococcus aureus (S. aureus)* strains. Gram-negative (*E. coli*) and Gram-positive (*S. aureus*) bacteria, represented by the numbers ATCC 25922 and 25923, respectively, are clinical strains utilized in this experiment. The bacteria used were grown in an autoclaved Petri dish that was imbued with a Lysogeny broth (LB) at pH 7.4, containing 0.5% yeast and 1% each of sodium chloride and tryptone. After applying the grown bacterial culture (60 μL) onto each agar plate with LB medium and 1.5% agar, the culture was equally distributed throughout the LB agar plates using a glass spreader that had been ethanol sterilized. After that, each LB agar plate was used to embrace 5 mg of the hydrogel sample, and all the plates were then placed on a bacterial lawn at 37 °C. A zone reader scale was used to measure the zones of inhibition 24 hours later, with a minimum count of 1 mm. In the middle of the circle was the zone reader's "0" reading. The inhibition zone (I_z), measured in millimeters, was the distance between the circular area's center and edge.

2.5.5. Drug loading and release. Initially, solutions of pectin (0.5 g in 50 mL DW) and PVA (0.5 g in 40 mL DW) were combined and stirred for two hours at 70 °C. Here, 0.0075 g of GO was sonicated for 30 minutes in 10 mL of DW, then added to the pectin/PVA mixed solution and stirred for an additional hour. The pectin/PVA/GO combination was mixed with 50 mg of LVX dissolved per 10 mL of DW, followed by the addition of 20 μL of APTES and glycerin each. After being shaken again for two hours, the resulting solution was poured onto the plastic Petri plates and left to dry at room temperature. The hydrogel filled with LVX was referred to as DPPG. The drug's release was observed at 37 °C and pH 7.4 (physiological conditions). In 200 milliliters of 1 M PBS solution, DPPG was added together with 8 grams of NaCl, 1.44 grams of Na_2HPO_4, 0.24 grams of KH_2PO_4, and 0.2 grams of KCl dissolved in autoclaved DW. A twin beam UV-visible spectrophotometer set to 291 nm was used to expose the solution every 10 minutes. The pure PBS solution served as the standard, and the quantity of LVX released was calculated using the standard calibration curve. Eqn (5)–(7) provided empirical models that were used to study the kinetics and mechanism of drug release:

$$M_t = M_o + K_o t \text{ (zero-order kinetic model)} \quad (5)$$

$$\ln\frac{M_t}{M_o} = n\ \ln t + \ln k \text{ (Korsmeyer-Peppas kinetic model)} \quad (6)$$

$$ft = Q = K_H \times t^{1/2} \text{ (Higuchi kinetic model)} \quad (7)$$

M_o is the total drug content, while M_t is the quantity of drug released at time "t." The rate constants are shown by K_H, k, and K_o.

2.6. *In vivo* analysis

2.6.1. Ethical approval. The animals (30 female albino mice) used in the *in vivo* study were treated in compliance with the guidelines set out in the Directive 2010/63 of the European Community Council. The Institutional Ethics Committee of Animal Experimentation and Care (IECACE) at NIH (National Institutes of Health) examined and approved the experimental protocol (No. F.1-5/ERC/2024). Every *in vivo* experiment was conducted in compliance with the instructions and globally recognized standards.

2.6.2. Cutaneous wound animal model. All mice weighing between 18 and 25 grams were sourced from the animal house facility at NIH in Islamabad, Pakistan. The mice in the wound-healing investigation were kept at 25 ± 2 °C and 45 ± 5% relative humidity. Prior to the experiment, they had unrestricted access to food and water, and they were given seven days to become used to their new surroundings. Three groups (A, B, and C) were made *via* the random selection of 10 mice of the same weight and age in each group, and wound treatment was carried out as follows:

Group A—Pyodine treatment (control).

Group B—PPG-7.5 treatment.

Group C—LVX-loaded DPPG treatment.

2.6.3. Excision wound infliction. Ketamine hydrochloride/xylazine (100/10 mg kg^{-1}) was injected into the peritoneal cavity of mice to induce anesthesia. The mice were shaved dorsally with an electric clipper, and the wound area was marked with methylene blue. An incision measuring 2–3 mm in depth and 5–6 mm in width was made using sharp scissors, toothed forceps, and a surgical blade. All surgical operations were carried out in sterile settings, and post-operative care was ensured. The animals were given treatment once daily.

2.6.4. Wound assessment. In the excision model, wounds were measured daily and documented with digital photographs. Healing was evaluated using transparent paper to find the wound size. The extent of wound healing in each group was

determined by calculating the wound contraction percentage using eqn (8).

$$\text{Wound contraction (\%)} = \frac{\text{Wound Area on day 0} - \text{Wound Area on day } n}{\text{Wound Area on day 0}} \times 100 \quad (8)$$

Here, n represents the day (*e.g.*, second, third, fourth, sixth, and seventh). For each wound surface area measurement, three or more animals were included, and the final outcomes were obtained as mean ± SEM (standard error of mean).

2.7. Statistical analysis

For statistical analysis, one-way ANOVA was performed using Origin Pro (8.5.1) software (Origin Lab Corporation, USA). Kinetic parameters related to drug release from hydrogels and swelling behavior were evaluated through linear fitting. Antibacterial and cytocompatibility results, presented as mean ± SD, were obtained from three independent experiments.

3 Results and discussion

3.1. Scheme

Different concentrations of GO were used to develop a series of GO-reinforced pectin/PVA/APTES/GO hydrogels. This approach allows for the systematic investigation of how different GO concentrations influence the structural, mechanical and functional properties of hydrogels. The proposed scheme for the pH-sensitive hydrogels is provided in Fig. 2. The dotted and bold lines emphasize the system's structural cohesion and connection, respectively, illustrating the links and interactions among the functional groups of different components. Initially, a composite hydrogel network was formed by integrating pectin and PVA. This provided a biocompatible and flexible hydrogel matrix, where strong intermolecular hydrogen bonding occurred between –OH and –COO^- groups on PVA and pectin, respectively. This synergistic approach improved the mechanical properties of pectin by forming a robust 3D porous structure. The introduction of the –NH_2 group from APTES further accelerated the binding between the pectin/PVA matrix and GO *via* covalent bonding; hence, enhanced crosslinking density and stability were achieved. The uniform distribution of GO within the polymeric matrix and its hydrogen bonding and ionic interactions with the functional groups and drug-loaded molecules created a unified and multi-tasking structure, which could be attributed to mechanical veracity, sustained drug release, and wound healing efficacy. The pictures of prepared hydrogels in current studies are also provided in Fig. 2.

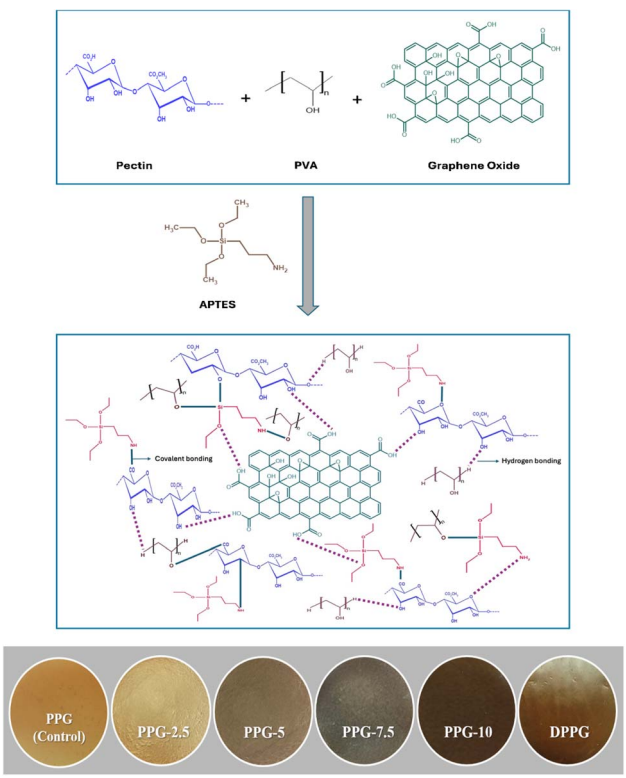

Fig. 2 A proposed scheme for the GO-reinforced pectin/PVA/APTES/GO hydrogel series and pictures of the synthesized hydrogels.

3.2. Structure, stability, phase, and surface morphology studies

3.2.1. FTIR. GO was prepared *via* the reported method and used to synthesize the GO-reinforced pectin/PVA/APTES/GO hydrogel series.[44] The characterization results of GO and the relative discussion, including Fig. S1, are provided in the SI, which confirmed the formation and stability of GO.

FTIR analysis was employed to confirm the functional groups of each component used in the synthesis of the hydrogel. The FTIR method validates how interactions have evolved to create hydrogel interfaces. Fig. 3(a) displays the FTIR spectra of individual hydrogel components, *i.e.*, pectin, PVA, APTES, and GO. A distinctive absorption peak for the –OH stretching and bending vibrations was seen in the pectin spectra around 3280–3600 cm^{-1} and 1025 cm^{-1}, respectively.[45] The absorption peaks at 2920 cm^{-1} and 1490 cm^{-1} were caused by the stretching and bending vibrations of polymer-linked C–H bonds. Moreover, stretching peaks at 1740 cm^{-1}, 1634 cm^{-1}, 1072 cm^{-1}, and 1139 cm^{-1} were found to correspond to C=O, COO^-, C–O–C, and CH–OH in the aliphatic cyclic secondary alcohol, respectively.[45] PVA exhibited –OH stretching band within the 3200–3550 cm^{-1} range. The –CH_2 wagging, C–H and C–O stretching bands were represented by the peaks seen at 1428 cm^{-1}, 2910 cm^{-1}, and 1094 cm^{-1}, respectively.[46] GO was recognized by the –OH stretching in the 3000–3700 cm^{-1} range. Peaks were observed at 1740 cm^{-1}, 1576 cm^{-1}, 1051 cm^{-1}, and 1316 cm^{-1} for C=O, C=C, C–O–C (epoxy), and C–O, respectively. Symmetric and asymmetric C–H stretching were represented by the peaks observed in the APTES spectrum, which were located at 2883 cm^{-1} and 2973 cm^{-1}, respectively. Peaks at 1094 cm^{-1}, 1000–1100 cm^{-1}, and 1441 cm^{-1} were detected, which indicate the vibrations for C–O, Si–O, and C–N stretching, respectively, but at 1389 cm^{-1}, CH_2 bending/wagging was recorded. These peaks verify that APTES contains silane, alkyl, amine, and ethoxy groups.[47]

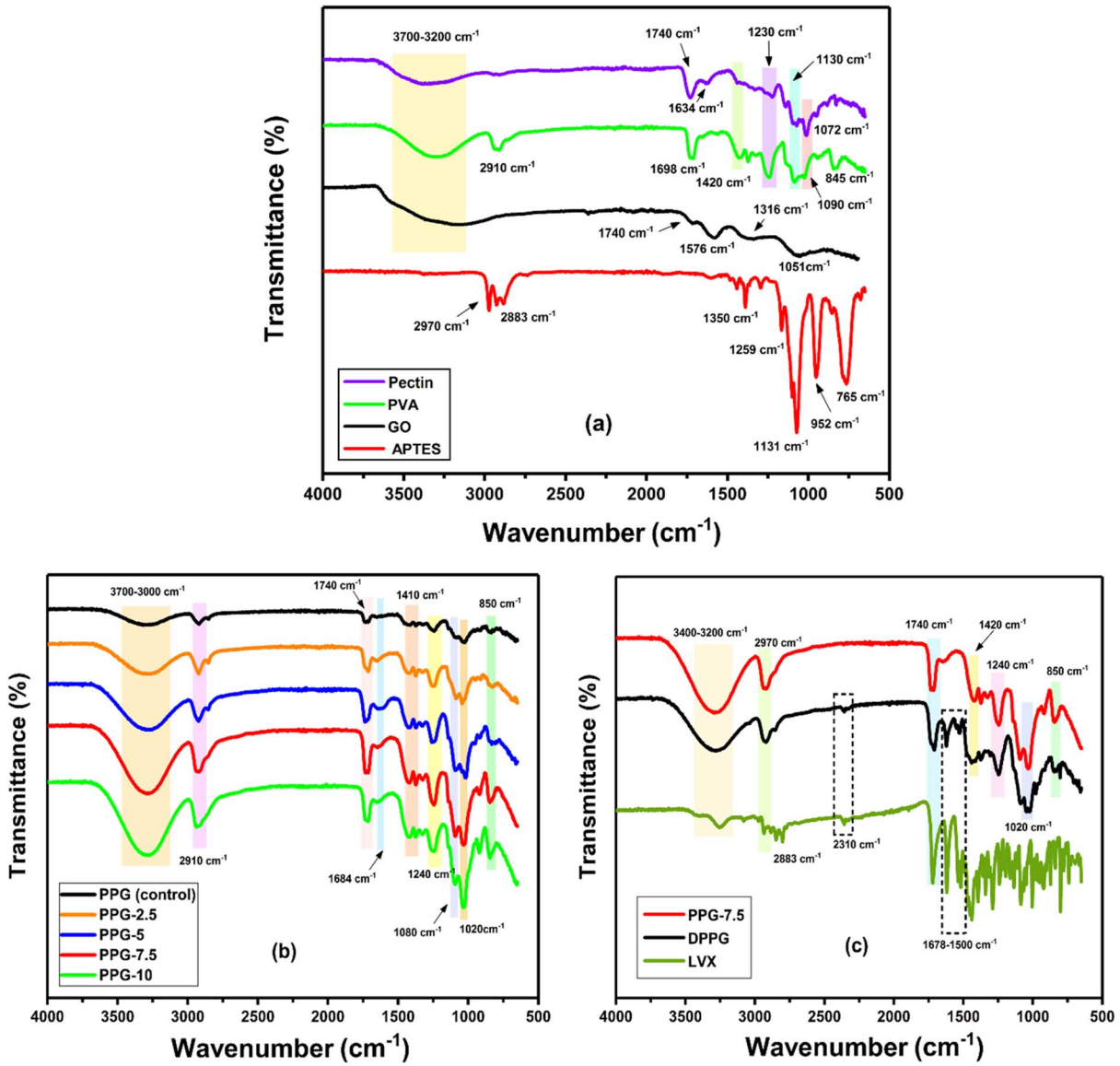

Fig. 3 FTIR spectra of the (a) individual components, (b) fabricated GO-reinforced pectin/PVA/APTES/GO hydrogels, and (c) pure LVX and LVX-loaded PPG-7.5 (DPPG).

Fig. 3(b) displays the FTIR spectra of the fabricated hydrogels (pectin/PVA/APTES/GO-PPG). The large stretching peaks appeared within the range of 3000–3600 cm^{-1} and were ascribed to the –OH groups found in certain hydrogel components, including GO, PVA, and pectin. The peak's broadness confirmed that hydroxyl groups were involved in hydrogen bonding. Additionally, the vibrational peaks associated with –OH bending were detected at 1374 cm^{-1}.[48] The polymer-linked C–H stretching and bending vibrations were observed at 2922 cm^{-1} and 1420 cm^{-1}, respectively. A prominent interaction between polymers and APTES was the formation of siloxane linkages (Si–O–Si), identified by an intense peak at 1020 cm^{-1} in all hydrogel formulations.[49] In pectin and GO, characteristic bands for C=O, C–O–C, $–COO^-$, and CH–OH were seen at 1730 cm^{-1}, 1086 cm^{-1}, 1645 cm^{-1}, and 1145 cm^{-1} on average. APTES's characteristic C–N peak was found at 1441 cm^{-1}. In pectin, PVA, APTES, and GO, the bands at 1526 cm^{-1} and 1081 cm^{-1} represented C=C and C–O, respectively. Comparable spectral peaks with variations in intensity, depending on hydrogel composition, were observed for the hydrogels, as shown in Fig. 3(b). The findings verified the existence of all functional groups within the hydrogels.

The FTIR spectrum of LVX showed characteristic peaks for O–H and N–H stretching in the range of 3600–3100 cm^{-1}. Peaks corresponding to C–H, C=O, and C–F stretching appeared at 2935 cm^{-1}, 1720 cm^{-1}, and 746 cm^{-1}, respectively. A peak at 1622 cm^{-1} was attributed to C=O stretching within the aromatic ring.[50] No peak shift was observed in the drug-loaded hydrogel (DPPG-7.5); however, compared with PPG-7.5, similar peaks appeared with reduced intensity and broadness. The spectral region between 1500 and 1678 cm^{-1} further confirmed LVX loading in DPPG, as shown in Fig. 3(c).

3.2.2. TGA. The hydrogels' thermal behavior was assessed using TGA. Each component of the hydrogel has an impact on the degradation pattern. Fig. 4(a) displays the TGA responses of GO-reinforced (0–10 mg) PPG and drug-loaded DPPG as a function of temperature. Three different phases of weight loss were seen in the thermogram of GO-reinforced hydrogels. The first step involved the removal of moisture content and the trapped solvent molecules at temperatures between 15 and 200 °C. The second step, which ranged from 200 to 280 °C, was related to side chain removal and decarboxylation inside the

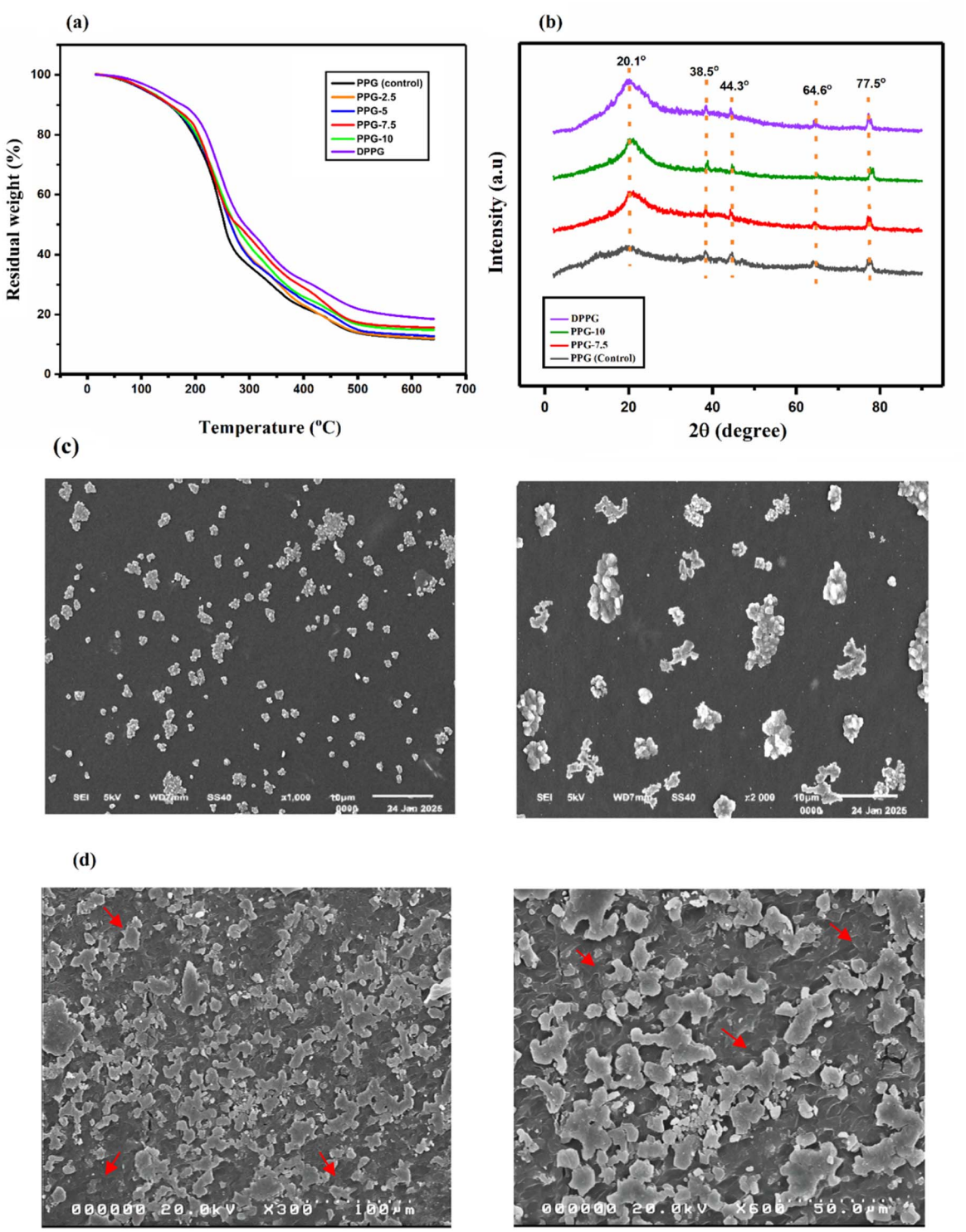

Fig. 4 (a) TGA thermograms, and (b) X-ray diffractograms of the GO-reinforced pectin/PVA/APTES/GO hydrogel blends. (c) SEM micrographs of PPG-7.5 at different magnifications. (d) SEM micrographs of DPPG (LVX-loaded PPG-7.5).

hydrogels. This might also be referred to as the initial degradation zone where polymer degradation began. The third stage, which showed the breakdown of the remaining polymeric backbones, spanned from 290 to 645 °C.[51] Additionally, the increase in GO concentration resulted in decreased hydrogel degradation. The strong carbon–carbon bonds in GO provide thermal stability; it will not lose much of its weight until temperatures rise over 500 °C. APTES also offers stability because of its silane groups and is likely to show decomposition at temperatures higher than 400 °C.[52]

According to the TGA results, the stability of hydrogels was closely correlated with the amount of GO since it had many binding sites, such as C═O, –OH and –COO^-, which consequently provide better hydrogel stability by forming strong intermolecular interactions. The TGA curve of LVX-loaded PPG-7.5 (DPPG) showed enhanced thermal stability, which was explained by the drug and hydrogel forming robust intermolecular connections. Each LVX molecule has one carbonyl, one fluorine and three nitrogen atoms, all of which contribute to the formation of intermolecular interactions with the groups in the hydrogel, resulting in improved stability.[53] Additionally, LVX adsorbs onto the GO surface *via* π–π interactions, increasing the interfacial bonding and load transmission. The hydrophobic regions of LVX may also stabilize the structure by interacting with non-polar sections of the hydrogel.[54] By increasing the crosslink density and reducing polymer chain mobility, these interactions produce a hydrogel network that is more compact, cohesive, and thermally stable. Table 2 displays the hydrogels' residual weights at various temperatures.

3.2.3. XRD. Fig. 4(b) displays the produced hydrogels' XRD data. The semi-crystalline nature of PVA was validated by the analysis, which showed a shoulder peak at $2\theta = 22.5°–22.7°$ and conspicuous peaks at $2\theta = 19.2°–20.5°$ (related to the (101) plane), while additional peaks at $2\theta = 11.2°$, 15.3°, 16.1°, 38.5 and 44.3° reflected various structural characteristics and hydrogen bonding within the polymer.[55] Meanwhile, pectin showed XRD peaks around 2θ values of 18.21°, 20.14°, 22.42°, 39.36°, 42.54°, 45.23°, 67.11° and 79.14°.[45] The formation of an amorphous hydrogel led to peak broadening and merging in the XRD pattern. Comparable amorphous interactions have been reported in the literature.[56]

The amount of GO in each blank hydrogel specimen varied (0, 7.5, and 10 mg), although they all had the same composition. The order and architecture within hydrogels were directly enhanced by hydrogen bonding and cross-linking between functional groups such as –OH, –COO^-, and C═O found in GO. The crystallinity caused by the chemical cross-linking also affected the intensity. PPG-10 exhibited higher intensity values, whereas lower intensities were seen in PPG (control). Amorphous hydrogels were produced because of the successful integration of all components, according to XRD patterns.

3.2.4. SEM. The SEM micrographs of PPG-7.5 and DPPG hydrogels are shown in Fig. 4(c) and (d), respectively. SEM micrographs of PPG-7.5 depicted the heterogeneous, porous, and uneven frameworks. By retaining moisture and allowing oxygen to pass through, this structure is well-suited for applications such as wound healing. Furthermore, channelized networks and multi-layered grooves (shown with red arrows) are visible, as displayed in Fig. 4(d). These surfaces are essential for drug loading and release because they increase the surface area of the hydrogel.[57] In comparison with PPG-7.5, the DPPG surface is denser, as is evident from the SEM images shown in Fig. 4(d). Additionally, the apparent multi-dimensional grooves provide a reservoir for solvent and drug molecules. The morphologies of DPPG and PPG-7.5 differ because LVX molecules were effectively loaded on DPPG, as shown in Fig. 4(d). Hence, the successful synthesis of hydrogel formulations and the efficient LVX loading on the hydrogels was confirmed by SEM micrographs.

Table 2 Residual weights of PPG and the GO-reinforced pectin/PVA/APTES/GO hydrogels at different temperatures

	Residual weight (%)					
Hydrogels	100 °C	200 °C	300 °C	400 °C	500 °C	600 °C
PPG (control)	95.41	78.58	36.14	22.28	13.83	12.15
PPG-2.5	95.57	79.92	39.29	23.04	14.06	12.37
PPG-5	95.84	80.05	38.74	24.71	14.93	13.15
PPG-7.5	95.79	80.53	42.86	25.86	16.71	15.01
PPG-10	95.87	82.13	45.66	28.99	17.40	15.83
DPPG	97.17	86.28	48.02	31.38	21.95	19.07

3.3. *In Vitro* studies

3.3.1. Biodegradation investigation. Biodegradable hydrogels are useful in biomedical applications since they do not need to be removed after the release of encapsulated therapeutic agents. The tuneable degradation of the hydrogel can also regulate the release of drugs from the hydrogel.[39] Furthermore, pectin and PVA have exceptional biodegradability and are responsible for the hydrogels' biodegradation capabilities. Hydrolysis, polymer breakdown, and solubilization are responsible for this degradation.[58] Pectin monomers are joined by glycosidic bonds that are readily broken down by a variety of enzymes to form short polysaccharide chains. These chains undergo further disintegration to be incorporated into the cellular metabolic pathways.[59] The biodegradation of GO-reinforced PPG hydrogel films was investigated for 21 days in PBS and in proteinase-K solutions; the results are shown in Fig. 5(a) and (b), respectively. The estimated biodegradation rates were found to be 93%, 89.07%, 84.86%, 83.27%, and 78% in PBS and 93.33%, 90%, 85%, 83.33% and 80% in proteinase-K medium for PPG (control), PPG-2.5, PPG-5, PPG-7.5, and PPG-10, respectively. The biodegradation information is given in Tables S1 and S2 of the SI.

Biodegradation results are conclusive that the weight loss of 3D hydrogels did not occur linearly over time; weight reduction was much quicker at the start, and the hydrogel broke down more slowly in PBS solution. In contrast, faster breakdown occurred in the enzymatic solution because of the availability of binding sites and free acetyl groups in pectin molecules. Consequently, proteinase-K broke down the glycosidic bonds that were present in the pectin.[60] Moreover, the addition and

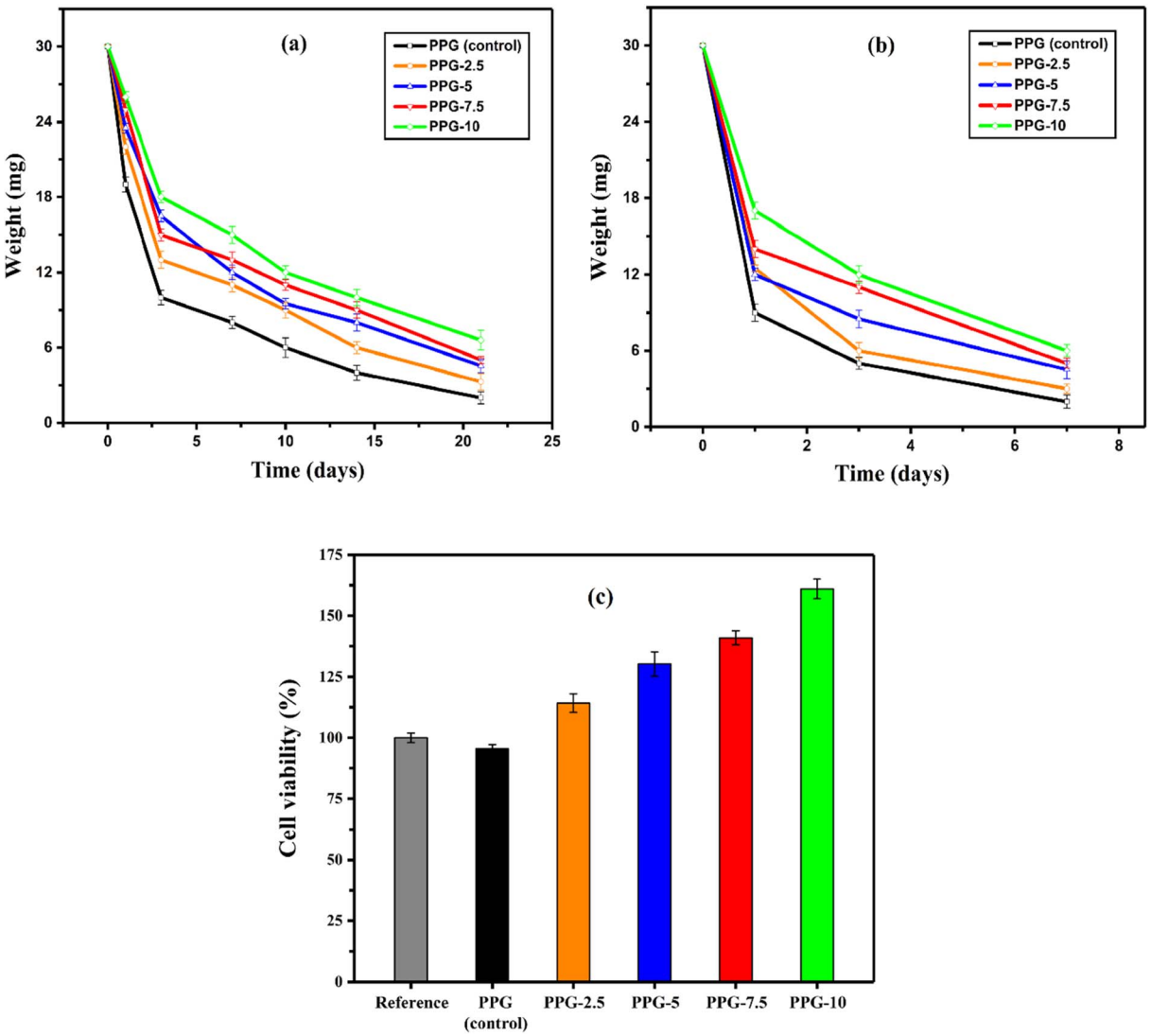

Fig. 5 *In vitro* biodegradation studies of the GO-reinforced pectin/PVA/APTES/GO hydrogels in (a) PBS and (b) proteinase-K. (c) Cell viabilities (%) of pectin hydrogels after 24 h. The data are represented with ± SD.

increase in the amount of GO showed an adverse effect on the hydrogel biodegradation in PBS and enzymatic solutions, which may be related to a comparative reduction in the available binding sites on pectin. The binding provided by the various groups on the GO surface may also be accountable for the increased stability in the hydrogel matrices.[61] Hydrolysis is the main process involved in the biodegradation of pectin-based hydrogels in an aqueous environment. The water molecules target the α-1,4-glycosidic linkages in pectin. Consequently, these linkages are broken and produce monomers and oligomers of galacturonic acids.

3.3.2. Cell viability investigation. Fig. 5(c) shows the cell viabilities of the reference (HEK-293 cells without hydrogel), PPG (control), PPG-2.5, PPG-5, PPG-7.5, and PPG-10 samples. Absorbance values were noted after 24 hours. Table 3 presents the statistical parameters derived from the cell line data. Enhanced cell multiplication in the presence of hydrogels, as is obvious from the findings, revealed their cytocompatibility and viability (Fig. S2–S7 in the SI). However, PPG-10 had the highest cell viability among all the samples, which indicated that the cell viability increased as the amount of GO increased. This may be related to GO's antibacterial and antioxidant qualities, which shield cells from infections and oxidative stress, while its vast

Table 3 Statistical parameters for the cell viability of GO-reinforced pectin/PVA/APTES/GO hydrogels

	Statistical parameters					
Samples	N	Average	SD	Sum	Median	Cell viability (%)
Reference	3	1.5848	0.0878	6.3391	1.6005	100
PPG (control)	3	1.5171	0.0793	4.5512	1.4968	95.73
PPG-2.5	3	1.7251	0.2372	5.1752	1.7263	108.85
PPG-5	3	1.9662	0.3654	5.8986	2.004	124.07
PPG-7.5	3	2.1273	0.1899	6.3818	2.1357	134.23
PPG-10	3	2.4309	0.2653	7.2927	2.4087	153.39

surface area and oxygen-containing functional groups encourage cell adhesion and growth.[62] Additionally, GO's capacity to imitate extracellular matrix structures produces an environment that is conducive to cell development.[63] The increased cell viability indicates the hydrogels' appropriateness for biomedical applications.

3.3.3. Swelling investigations

3.3.3.1. In distilled water (DW). The primary cause of hydrogel swelling is the migration of liquid solvents into the polymeric matrix from external media. The pectin-based hydrogel blends' time-dependent swelling percentages in DW are displayed in Fig. 6(a). The hydrogel samples clearly showed the greatest swelling at 120 minutes, which is known as the swelling equilibrium. All pectin hydrogels demonstrated excellent swelling characteristics because the hydrophilic groups in pectin form hydrogen bonds and electrostatic interactions with water molecules, allowing pectin to absorb and hold substantial amounts of water.[64] All hydrogel formulations, except PPG

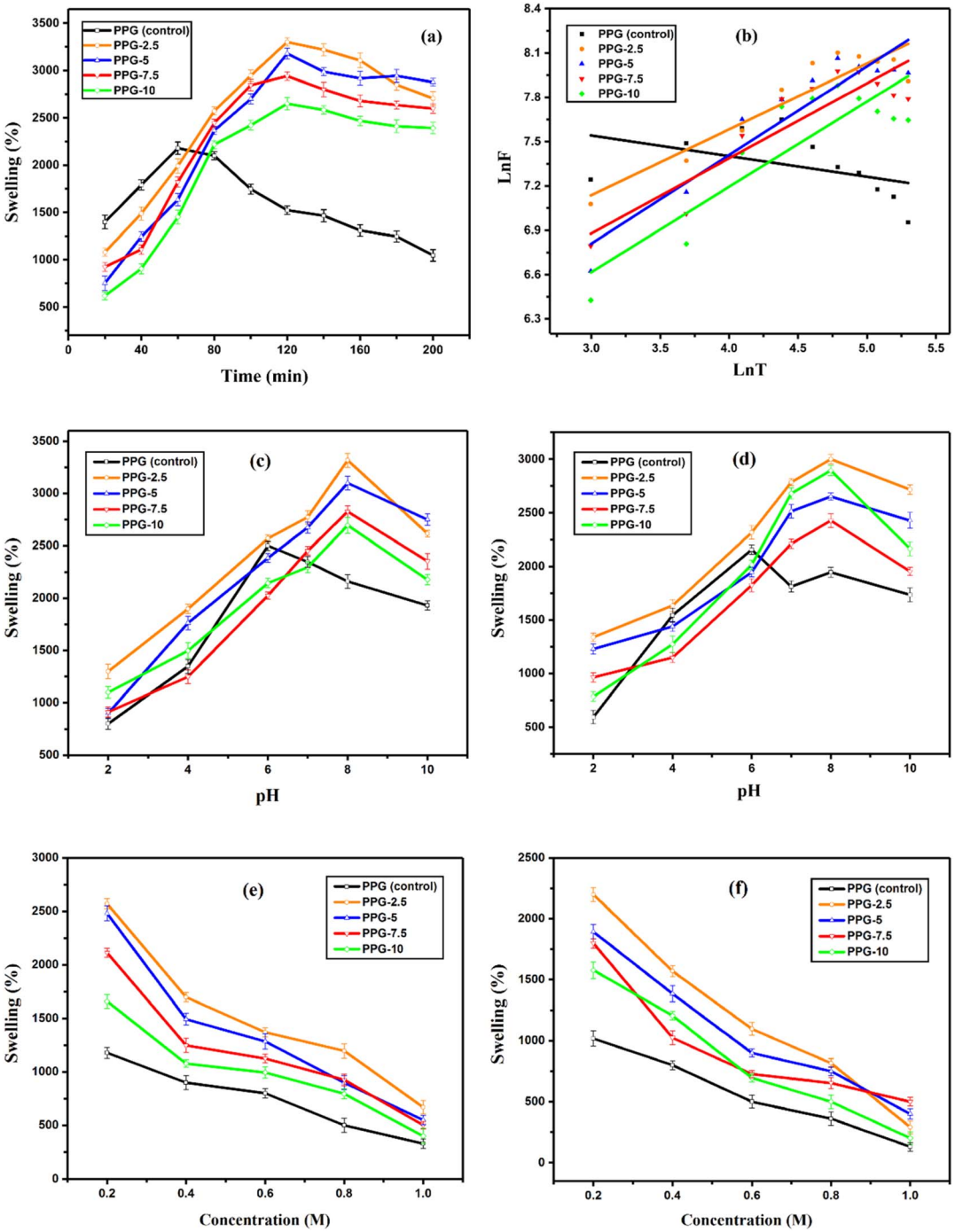

Fig. 6 (a) DW swelling pattern of hydrogels. (b) Diffusion parameter calibration curves. Hydrogel swelling patterns in (c) non-buffer solutions, (d) buffer solutions, (e) NaCl, and (f) $CaCl_2$.

Table 4 The calculated diffusion parameters for the swelling of GO-reinforced pectin/PVA/APTES/GO hydrogels

	Hydrogel samples				
Parameters	PPG (control)	PPG-2.5	PPG-5	PPG-7.5	PPG-10
Adj. R-square	0.122	0.844	0.872	0.792	0.740
R-square (COD)	0.221	0.861	0.886	0.815	0.769
Slope (n)	−0.139	0.345	0.499	0.407	0.477
Intercept	7.961	5.799	5.011	5.356	4.886
k	2963.04	632.67	291.59	418.92	270.08

(control), exhibited a steady increase in swelling percentage over time, with slight variations. In contrast, PPG (control) showed a decrease in swelling over time due to the absence of filler, which led to lower mechanical strength and gradual disintegration during swelling.

At 120 minutes, PPG-2.5 exhibited the highest swelling percentage of 3300%, whereas PPG (control) showed the lowest swelling percentage of 1523%. The existence of cross-linking capabilities in GO may be the reason for the observed decrease in swelling % with an increase in GO quantity. GO is comprised of a range of moieties, such as OH, COOH, and C=O, and helps to improve the binding affinities within the hydrogel architecture. Since GO is directly related to the hydrogels' cross-linking points, it enhanced the compactness and resulted in less swelling.[65] Diffusion is an important phenomenon in swelling; it is a process that causes swelling by allowing water or a solvent to migrate inward into hydrogel networks. The diffusion phenomenon is represented by eqn (4).[66] The calibration curves derived from the "LnF" *vs.* "LnT" plots are displayed in Fig. 6(b), and Table 4 gives the diffusion parameters' numerical values.

The diffusion model, transport and release mechanism of solvents, and the drug molecules in hydrogel matrices are described by the value of the swelling exponent "*n*". The values of "*n*" in Table 4 indicate stereo-selective quasi-Fickian diffusion, as they are consistent with $n < 0.5$.

3.3.3.2. In non-buffer and buffer solutions. If a pectin hydrogel has ionizable functional groups like –OH and –COOH in its structure, it will be more sensitive to pH changes.[67] Changes in the environment cause an imbalance in the charges within the polymeric chains present in the hydrogel network. The hydrogels in the current studies are regarded as pH sensitive because they demonstrate pH-dependent swelling behavior. Fig. 6(c) illustrates how hydrogels swell in non-buffer solutions. The greatest swelling was seen in a basic medium at pH 8, whereas all the hydrogels had decreased swelling volumes in acidic solutions. The carboxyl groups in pectin stay protonated in acidic environments (low pH), which increases hydrogen bonding and decreases electrostatic repulsion between the polymeric chains.[68] The compact and condensed hydrogel structure reduces swelling by limiting the mobility of polymeric chains and lowering water absorption. Alternatively, these carboxyl groups deprotonate in basic circumstances (high pH), which increases electrostatic repulsion and promotes swelling.[69] Furthermore, the amine groups in APTES also show pH-dependent ionization. At higher pH levels, the amines become less protonated, reducing crosslinking density and allowing the network to expand.[70] Additionally, the polymeric chains have charged zones over pendant chains at basic pH, which resist one another and enhance swelling.[71] The osmotic pressure and the solution's molar concentration are related as well. Deprotonation causes the molar concentration of –OH ions, which are present in water, pectin, PVA, and GO, as well as –COO ions, which are present in pectin and GO, to climb in the solution as the pH increases.[72] Consequently, this increases the hydrogel's internal osmotic pressure, which results in larger swelling percentages. PPG-2.5 showed the most swelling at pH 8 (3317%), whereas PPG (control) showed the least amount of swelling (2162%).

Fig. 6(d) illustrates how hydrogels swell when immersed in buffer solutions. Interestingly, differences in ionic concentration account for the varying swelling levels observed in buffer and non-buffer solutions at the same pH. A higher ionic strength in buffers reduces the osmotic pressure difference between the hydrogel and its environment, leading to lower water uptake and network swelling.[73] Moreover, the hydrogels' buffer swelling trend is comparable to that of non-buffers, with

Table 5 Swelling percentages of GO-reinforced pectin/PVA/APTES/GO hydrogels in DW, buffer, and non-buffer solutions

	% Swelling of hydrogels in DW				
Time (min)	PPG (control)	PPG-2.5	PPG-5	PPG-7.5	PPG-10
20	1398	1080	753	924	618
40	1790	1488	1244	1109	906
60	2179	1991	1633	1821	1450
80	2099	2572	2366	2445	2217
100	1745	2945	2701	2845	2422
120	1523	3300	3179	2940	2650
140	1464	3219	2987	2800	2584
160	1309	3106	2917	2679	2469
180	1245	2850	2943	2635	2412
200	1047	2705	2877	2598	2392
	% Swelling of hydrogels in buffer				
pH	PPG (control)	PPG-2.5	PPG-5	PPG-7.5	PPG-10
2	594	1338	1229	963	784
4	1543	1634	1439	1148	1273
6	2156	2317	1946	1825	2016
7	1813	2785	2513	2211	2680
8	1945	3000	2651	2426	2894
10	1735	2716	2427	1953	2165
	% Swelling of hydrogels in non-buffer				
pH	PPG (control)	PPG-2.5	PPG-5	PPG-7.5	PPG-10
2	805	1310	900	912	1104
4	1347	1898	1763	1248	1498
6	2500	2570	2385	2026	2145
7	2347	2773	2675	2451	2296
8	2162	3317	3100	2826	2695
10	1930	2616	2757	2353	2178

pH 8 giving the highest swelling. PPG-2.5 showed the most swelling (3000%) in buffers, whereas PPG (control) showed the least swelling (1945%) at pH 8. Pectin hydrogels are especially helpful in applications like drug administration because of their pH-dependent swelling characteristics, which allow them to release therapeutic compounds in response to certain pH conditions, such as those in various gastrointestinal tract regions. Table 5 shows the percentage swelling of hydrogels in DW with respect to time, as well as in buffer and non-buffer solutions at different pH values.

3.3.3.3. In ionic solutions. The swelling behaviors of polymeric hydrogels are affected by molar concentrations, ion types and charge densities;[74] thus, NaCl and $CaCl_2$ solutions (0.2, 0.4, 0.6, 0.8, and 1 M) were prepared. Despite having the same anion (Cl^{-1}), the two electrolyte solutions have differing cations (Na^{+1} and Ca^{2+}), thus they have different charge-to-size ratios. Hydrogel swelling trends in NaCl and $CaCl_2$ are depicted in Fig. 6(e) and (f), respectively. A clear decrease in swelling pattern was observed as ionic concentration and charge density increased. In 0.2 M NaCl and 0.2 M $CaCl_2$, PPG-2.5 showed the largest swelling percentages of 2570% and 2198%, respectively. Additionally, the swelling percentages reduced as the molar concentrations of $CaCl_2$ and NaCl increased. This pattern can be explained by three factors. First, the hydrogel's NH_2 and COOH groups form metal complexes with polyvalent cations like Ca^{+2}, resulting in compact frameworks with reduced swelling volumes.[10] Another contributing factor is the restricted movement of metal ions due to their binding with negatively charged regions within polymer chains. Additionally, strengthened electrostatic shielding between charged groups reduces internal osmotic pressure and further limits the hydrogel swelling.[74]

However, because of the interactions between the functional groups, the increase in GO amount promotes stability, compactness, and ultimately reduces swelling. Compared to $CaCl_2$, larger swelling volumes are seen in NaCl. For instance, PPG-7.5 showed 1248% and 1025% swelling in 0.4 M NaCl and $CaCl_2$ solutions, respectively, which was due to the difference in ionic charge. Because of inter-chain connections, a high ionic charge causes compactness in the hydrogel structure. The bigger ions were also unable to enter the polymeric network.[57]

3.3.4. Antibacterial activity investigation. Fig. 7 illustrates the antibacterial activity of all GO-reinforced pectin/PVA/APTES/GO hydrogels against *S. aureus* and *E. coli*, while the evaluated I_z values are provided in Table 6. However, amongst all hydrogel samples, the antibacterial activity of PPG-7.5 was comparatively stronger against both strains of bacteria, with inhibition zone (I_z) values of 5.0 ± 0.01 mm for *S. aureus* and 7.0 ± 0.02 mm for *E. coli*. Overall, all hydrogels had higher antibacterial efficacy for Gram-negative bacteria.

The observed antibacterial activity of pectin-based hydrogels could be linked to their ability to generate pores in bacterial membranes, leading to cytoplasmic leakage and cell death. The carboxylic groups (–COOH) in pectin deprotonate upon interaction with bacterial cells, releasing H^+ ions that alter the pH and disrupt the cell wall, while carboxylate ions (COO^-) inhibit cellular activities by binding with positively charged species in the bacteria.[75] Moreover, the bactericidal action of hydrogels was enhanced in the presence of GO, which may have generated reactive oxygen species (ROS) and physically disrupted the bacterial membranes *via* its sharp edges and charge interactions.[76,77]

The stronger antibacterial action against Gram-negative bacteria may be due to variations in their cell wall structures. Gram-negative bacteria possess a thinner peptidoglycan layer and an outer membrane that may be more susceptible to disruption by GO and other reactive components in the hydrogel. GO has been reported to generate oxidative stress and cause membrane damage, which may be more effective against Gram-negative than against Gram-positive species.[76,77] The irregular

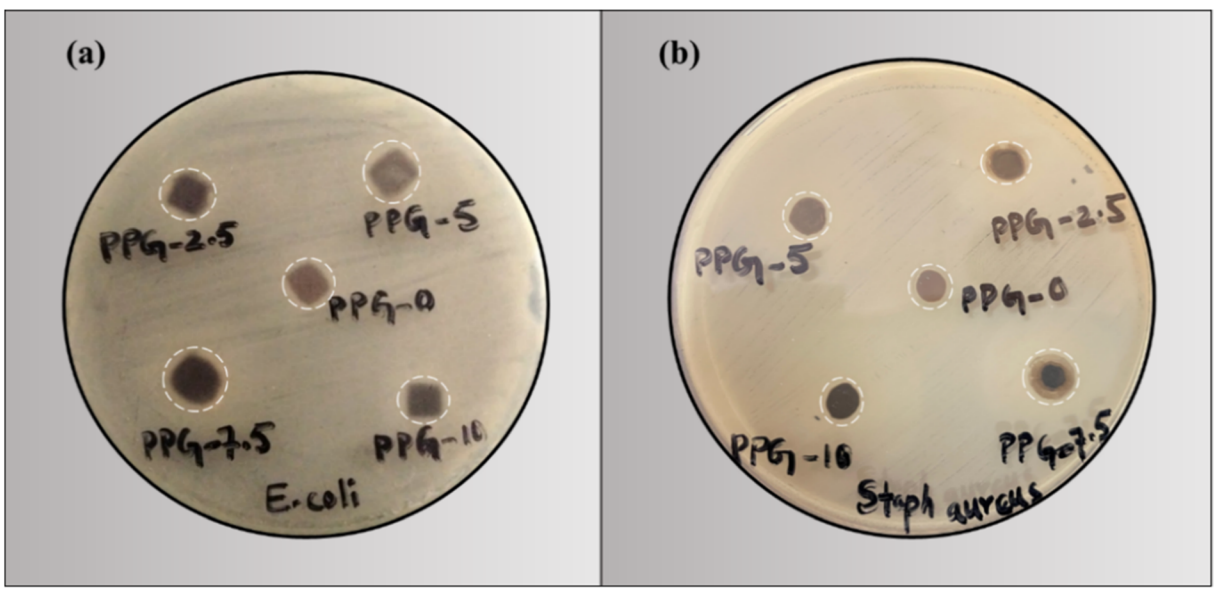

Fig. 7 Antibacterial activity investigation performed for the GO-reinforced pectin/PVA/APTES/GO hydrogels against (a) *E. coli* and (b) *S. aureus*.

Table 6 Inhibition zone (I_z) values of GO-reinforced pectin/PVA/APTES/GO hydrogels against *E. coli* and *S. aureus*, presented as mean ± SD

	I_z (mm)				
Bacteria	PPG (control)	PPG-2.5	PPG-5	PPG-7.5	PPG-10
E. coli	4.0 ± 0.02	4.8 ± 0.06	6.0 ± 0.04	7.0 ± 0.02	5 ± 0.02
S. aureus	2.7 ± 0.03	3.4 ± 0.02	4.1 ± 0.05	5.0 ± 0.01	3.0 ± 0.04

antibacterial activity is likely due to GO dispersion and possible agglomeration at higher concentrations. This affects surface area and contact-based antibacterial action. Variations in surface morphology, hydrogel swelling, diffusion rate, interactions between the bacterial population, hydrogel surface, and hydrogel density may also influence bacterial interaction.

3.3.5. Drug (LVX) release investigation. Owing to the favorable swelling performance and other intact activities, including antibacterial activity, stability and cell viability, PPG-7.5 was chosen for loading the LVX drug. The loaded sample was denoted as DPPG. The standard calibration curve for LVX is presented in Fig. 8(a), while the plot of LVX release from DPPG in PBS is provided in Fig. 8(b). The drug was steadily released from the hydrogel, as shown in Fig. 8(b), and equilibrium was reached after 210 minutes; 91.44% of drug release was estimated in PBS solution at pH 7.4 in 3.5 h. Time-dependent drug release data are provided in the SI in Table S3. Gazzi *et al.* reported that pectin hydrogels loaded with imiquimod showed 63% drug release within 2 hours.[78] The drug release in the current work was also found to be more pronounced when compared with our recently reported work, where a hydroxyapatite-reinforced pectin-based hydrogel released 88.57% of doxycycline within the same time frame and pH.[79] Further comparison with reported literature indicated that the hydrogel in the current work demonstrated a slightly slower release, with 91.44% of LVX released over 3.5 hours. This suggests that the incorporation of APTES and GO may have contributed to a denser network structure, slowing the drug diffusion rate. The more gradual release profile implies better control over drug delivery. Such sustained release may be beneficial for a prolonged therapeutic effect.

Initially, the LVX release rate was higher, but it slowed down afterward. The main factors that are responsible for the release of a drug from the host hydrogels are hydrogen bonding, van der Waals interactions, and condensation processes.[73] Three main mechanisms, *i.e.*, swelling, diffusion, and erosion, are considered to regulate the release of a drug from the hydrogel.[67] The faster release of the drug at the start occurred due to a swelling-controlled drug release mechanism.[56,80] Diffusion-controlled release is the mechanism responsible for continued drug release once the swelling equilibrium is established. In diffusion-controlled drug release, the release rate remains constant and does not depend on concentration gradients or polymer matrix properties.[66] In the current work, the presence of GO inside the hydrogel matrix was responsible for the regulated release of LVX from DPPG.

The drug release followed zero-order, Higuchi, and Korsmeyer-Peppas kinetic models, as shown in Fig. 8 (c–e), and the evaluated kinetic parameters for all models are provided as inset tables. The controlled release of LVX from the hydrogel was confirmed using the K_o and R^2 values obtained from the linear plots of the models. The R^2 value > 95 indicates that the LVX release data fit the models well. The K_o values for zero order, Higuchi, and Korsmeyer-Peppas models were evaluated to be 0003, 6.051, and 0.452, respectively. This kinetic data further confirmed that the drug release was governed by a time-dependent diffusion-controlled mechanism.[72]

3.4. *In Vivo* wound healing studies

The biocompatibility, moisture retention, gel-forming ability, anti-inflammatory properties, antimicrobial activity, promotion of cell growth, and the ability to deliver drugs locally make pectin hydrogels useful for wound healing applications.[81] Additional bioactive substances can be added to formulations to increase their efficacy even more. These hydrogels provide an effective, safe, and biocompatible means to promote tissue regeneration and wound healing.[82] They have been shown in recent research to be beneficial in encouraging skin regeneration, especially in burn wounds and other skin lesions.[83] Contraction or wound restoration is the reduction of the wound area and is mostly determined by the extent and nature of the injury, vital health, and tissue-repairing ability.[84] In pectin-based hydrogels, pectin aids the wound healing process by creating a moist environment that speeds up tissue regeneration and reduces scarring. Its natural biocompatibility supports cell adhesion and growth, especially fibroblasts and keratinocytes. Pectin also helps to maintain the hydrogel's structure and has mild antimicrobial and anti-inflammatory effects, which protect the wound and promote faster healing.[81]

Herein, we have evaluated the efficacy of synthesized hydrogels (PPG-7.5 and DPPG) for their *in vivo* wound healing activity using the excision wound model. DPPG was made by loading 50 mg of LVX drug on the PPG-7.5 hydrogel. Fig. 9 (a–c) displays pictures and a quantitative analysis of the wound-healing rate using different dressings on the 0th, 1st, 3rd, 5th, and 7th days of treatment. The observed findings demonstrated accelerated wound healing in group B and C animals, where PPG and DPPG dressings were employed as compared to the control group A. In contrast to 20% healing in the control group treated with simply pyodine, up to 60–63% wound healing was observed in the DPPG group and 33–35% in the PPG-7.5 group within the first three days. This study also validated that the wounds were healed up to 98.3% and 67% on day 5 using DPPG and PPG-7.5 hydrogels, respectively, while in the control group, the healing was found to be 25% within this time span.

The PPG-7.5 hydrogel group significantly increased the rate of wound healing, achieving 75% healing on day 7, whereas

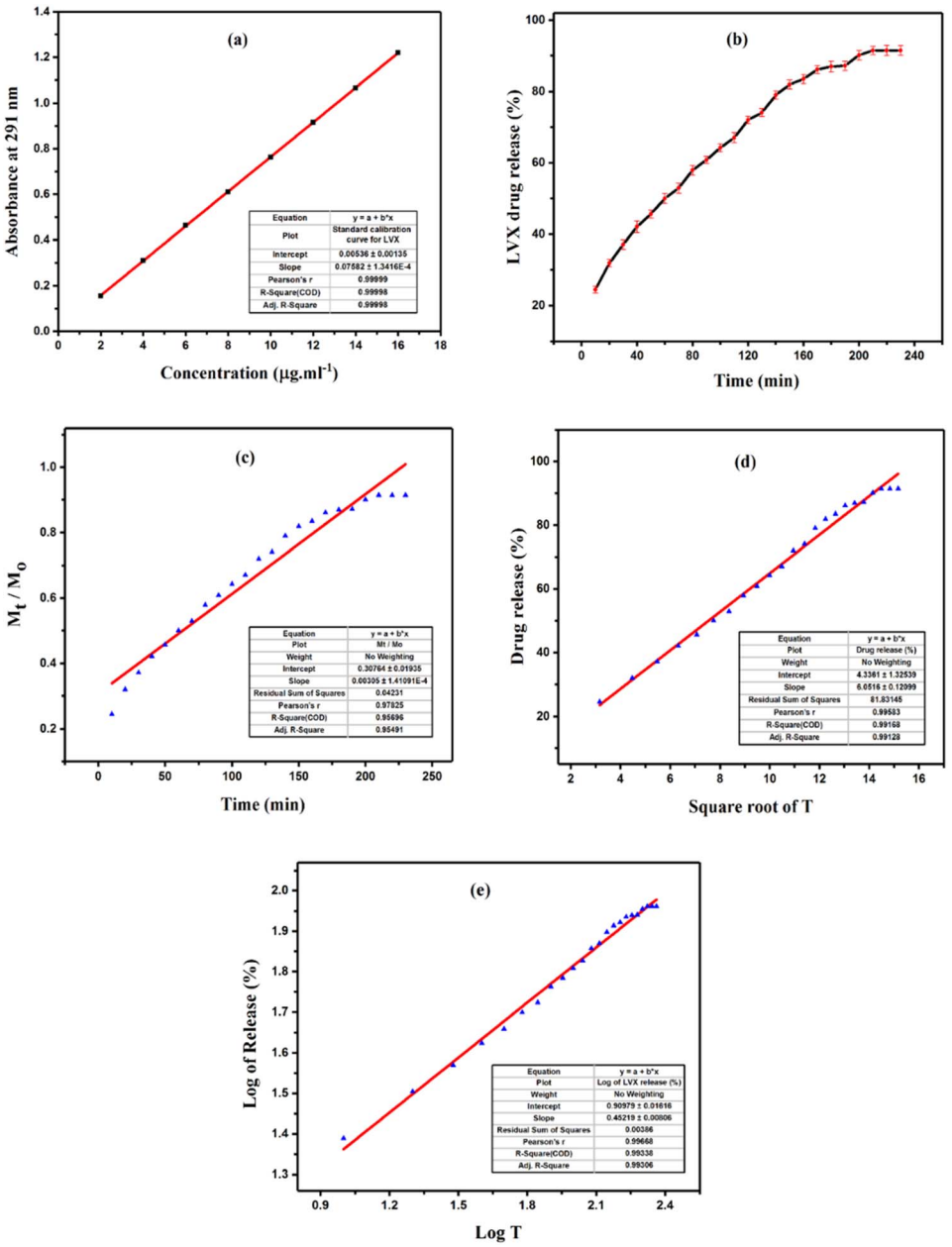

Fig. 8 (a) Standard calibration curve for LVX. (b) *In vitro* LVX release in PBS at pH 7.4. (c–e) Zero-order, Higuchi, and Korsmeyer-Peppas kinetic models, respectively, with inset tables showing the corresponding kinetic parameters.

surprising results were obtained with DPPG, as it completely (100%) healed the wound on the 7th day. This might be due to cell migration and proliferation, which are promoted by the hydrogel's extracellular matrix-like environment for the wound. In addition, the porous structure, controlled swelling behavior and tunable physicochemical properties of the hydrogel ensured sustained drug release from DPPG by regulating diffusion and degradation rates.[85] The degree of reduction of the wound area at the same time was as follows: DPPG > PPG-7.5 > control. While the control group displayed inflammation, PPG-7.5 and DPPG demonstrated no evidence of inflammation.

Wound healing *via* hydrogels follows the natural stages of hemostasis, inflammation, proliferation, and remodeling, with hydrogels actively enhancing each phase. During hemostasis, hydrogels provide a moist, adhesive barrier that aids clot formation and stabilizes the wound site. In the inflammatory phase, they support immune cell activity to clear debris and can deliver antimicrobial agents to reduce infection and excessive inflammation. In the proliferative phase, hydrogels maintain a hydrated environment that promotes fibroblast proliferation, collagen deposition, angiogenesis, and re-epithelialization, facilitating granulation tissue formation. Finally, during remodeling, hydrogels assist in extracellular matrix reorganization and collagen maturation, improving tissue strength and minimizing scarring. Their tunable properties also allow the incorporation of growth factors and bioactive molecules to

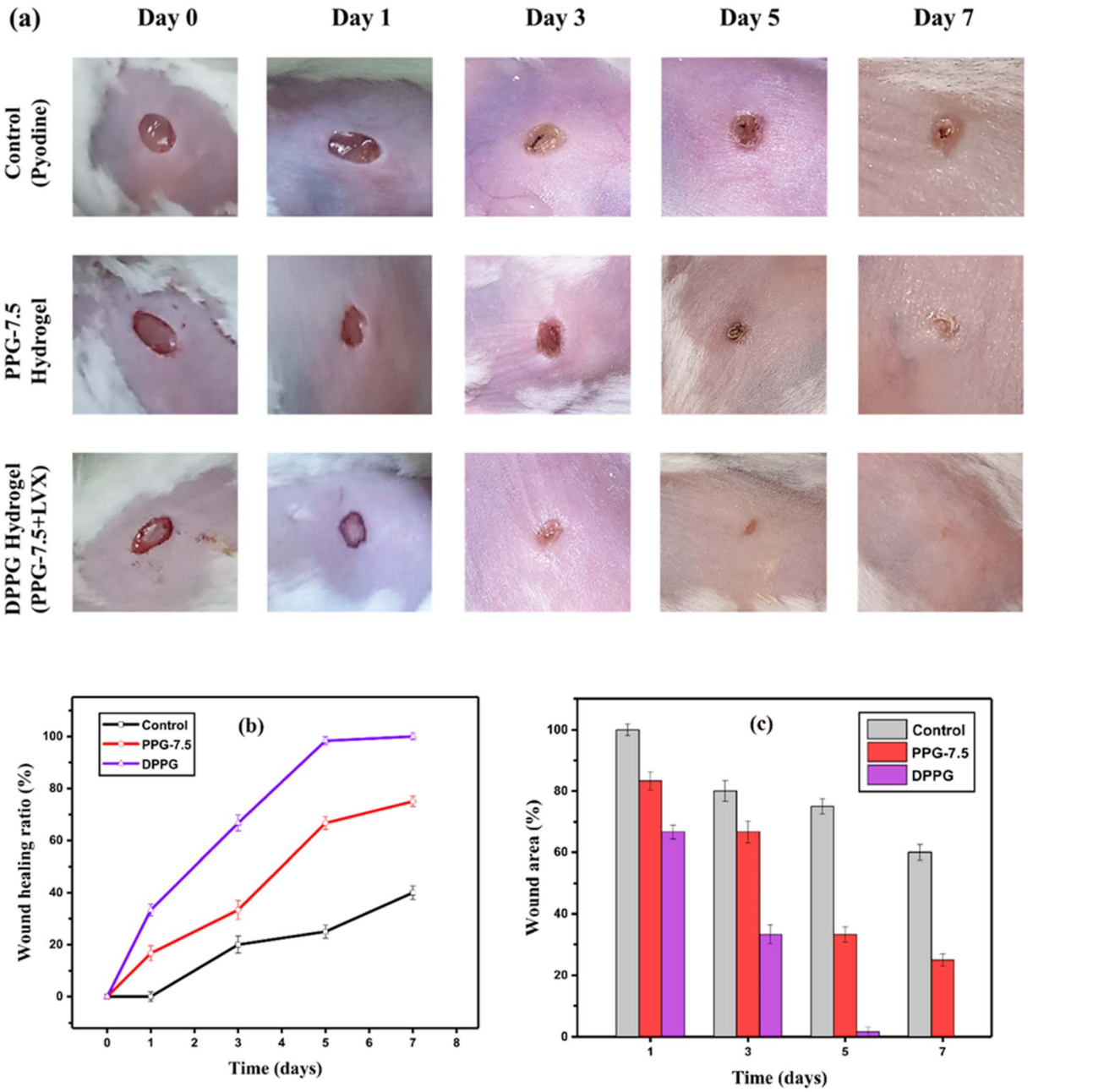

Fig. 9 (a) Images depicting wounds treated with the PPG series (GO-reinforced pectin/PVA/APTES/GO hydrogels) over a 7-day period. (b) The wound healing ratio as a function of time. (c) Quantitative analysis of wound contraction during the healing process.

further accelerate healing and tissue regeneration throughout these stages.[86–88]

Previous studies indicated that a hydrogel dressing achieving over 50% wound closure within 14 days reflects its effective design.[89] For instance, a simvastatin-loaded alginate-pectin hydrogel film attained approximately 99% wound closure in streptozotocin-induced diabetic rats after 21 days, markedly outperforming the control groups.[90] In one research, pectin-based hydrogels significantly improved the wound healing in male Wistar albino rats with burn injuries, as compared to untreated rats, and these effects were further intensified by the addition of plant extracts and iodine.[81] In another study, allantoin-enriched pectin hydrogels demonstrated wound healing of almost 71.43% in 15 days, where compared to rats treated with lesser concentrations, diabetic rat models treated with 5% pectin hydrogel showed greater rates of re-epithelialization and a quicker reduction in wound size.[91] These findings collectively highlight pectin's strong potential as a wound healing agent, demonstrating enhanced wound closure, re-epithelialization and accelerated healing, particularly when pectin is combined with therapeutic agents. The wound healing results of DPPG, in current studies, were also found to be more pronounced than those obtained in our previous wound healing studies using chitosan-based coatings

on surgical sutures, where complete healing was observed in 12 days.[92] GO-reinforced hydrogels were also reported for their *in vivo* wound healing performance. In a study on a chitosan composite hydrogel reinforced with functionalized GO, *in vivo* evaluation on full-thickness excision wounds in rats revealed that the GO-reinforced hydrogel markedly accelerated wound healing, achieving a closure rate of 92.2% within 21 days.[93] In another study, a hydrogel combining GO and N-acetyl cysteine (NAC) within a gelatin matrix was developed. The NAC-GO-Gel group achieved an 86.6% wound closure in 14 days, outperforming non-hydrogel groups.[94] Compared to the reported literature, the wound healing results in the present study are more surprising: DPPG shows excellent performance with 100% wound healing within a very short period of 7 days; hence, it could be considered a promising candidate for wound dressing application.

4 Conclusions

A solution casting approach was used to synthesize GO-reinforced pectin/PVA/APTES/GO hydrogels. In the hydrogel matrix, pectin served as a biocompatible base, while PVA improved mechanical strength and flexibility. APTES acted as a crosslinker, enhancing structural stability and controlling swelling. GO reinforced the network, enabling sustained drug release and antibacterial activity. Together, these components contributed to the hydrogels' overall performance. FTIR analysis confirmed the presence of functional groups from each hydrogel component, while XRD results indicated the amorphous nature of the hydrogels. SEM and TGA proved their porous morphology and thermal stability, respectively. The hydrogels exhibited good swelling performance, biodegradability, antibacterial activity and cell viability. The amount of GO had an inverse relationship with the extent of swelling, and maximum swelling (3300%) in DW was obtained with a low GO content. The pH sensitivity of the hydrogel was evaluated using both buffer and non-buffer media. Maximum swelling occurred at pH 8 in both cases, with higher swelling observed in the non-buffer solution (3317%) compared to the buffer solution (3000%). These findings indicate that the produced hydrogels could be used for applications involving controlled drug release. The controlled drug release studies revealed that an equilibrium was achieved after 210 minutes, and 91.44% LVX was released from DPPG in 3.5 hours. The Korsmeyer-Peppas, Higuchi, and zero-order kinetic models were used to validate a time-dependent, diffusion-controlled drug release mechanism. In addition, DPPG dressing, when applied to incision wounds on albino mice, showed surprising results of 100% healing within a week. This could be ascribed to the biocompatibility of the hydrogel and its cellular proliferation, migration, and moisture retention abilities, which in turn promoted tissue regeneration. Overall, the findings indicated the potential candidacy of the synthesized hydrogels for use in sustained drug release in drug delivery systems for the urinary tract and as dressings/bandages for the healing of wounds.

Author contributions

Hirra Manzoor – investigation, formal analysis, software, data curation, writing—original draft, writing—review and editing. Nasima Arshad – supervision, conceptualization, methodology, project administration, resources, validation, visualization, writing—original draft, writing—review and editing. Muhammad A. U. R. Qureshi – validation, methodology. Sher Qadar – software.

Conflicts of interest

There are no conflicts to declare.

Data availability

Data will be made available on request.

Supplementary information (SI): GO characterization description and related references; (a) FTIR spectrum (b) TGA thermogram and (c) XRD spectra of graphene oxide (GO) (Fig. S1); residual weight of GO-reinforced pectin/PVA/APTES/GO hydrogels in PBS solution with respect to time (Table S1); residual weight of GO-reinforced pectin/PVA/APTES/GO hydrogels in proteinase-K solution with respect to time (Table S2); drug release data of GO-reinforced pectin/PVA/APTES/GO hydrogel in PBS solution at pH 7.4 (Table S3); picture of cell viability analysis of the reference, PPG (control), PPG-2.5. PPG-5. PPG-7.5, and PPG-10 (Fig. S2–S7). See DOI: https://doi.org/10.1039/d5ra08329j.

Acknowledgements

We would like to express our gratitude to laboratory facilities of Allama Iqbal Open University for making this research possible. We also acknowledge the National Institute of Health, Islamabad, for enabling the *in vivo* trials. There was no financial support or funding for this research project from the public or private sectors.

References

1 M. Kumar, A. R. Hilles, S. H. Almurisi, A. Bhatia and S. Mahmood, Micro and nano-carriers-based pulmonary drug delivery system: Their current updates, challenges, and limitations – A review, *JCIS Open*, 2023, **12**, 100095, DOI: 10.1016/j.jciso.2023.100095.

2 M. Bustamante-Torres, D. Romero-Fierro, B. Arcentales-Vera, K. Palomino, H. Magaña and E. Bucio, Hydrogels classification according to the physical or chemical interactions and as stimuli-sensitive materials, *Gels*, 2021, 7(4), 182, DOI: 10.3390/gels7040182.

3 W. Xu, F. A. Burni and S. R. Raghavan, Reversibly Sticking Metals and Graphite to Hydrogels and Tissues, *ACS Cent. Sci.*, 2024, **10**(3), 695–707, DOI: 10.1021/acscentsci.3c01593.

4 M. Mahinroosta, Z. Jomeh Farsangi, A. Allahverdi and Z. Shakoori, Hydrogels as intelligent materials: A brief review of synthesis, properties and applications. Mater,

Today Chem., 2018, **8**, 42–55, DOI: 10.1016/j.mtchem.2018.02.004.

5 B. Liu and K. Chen, Advances in hydrogel-based drug delivery systems, *Gels*, 2024, **10**(4), 262, DOI: 10.3390/gels10040262.

6 Y. Xu, J. Hu, J. Hu, Y. Cheng, X. Chen, Z. Gu and Y. Li, Bioinspired polydopamine hydrogels: Strategies and applications, *Prog. Polym. Sci.*, 2023, **146**, 101740, DOI: 10.1016/j.progpolymsci.2023.101740.

7 T. C. Ho, C. C. Chang, H. P. Chan, T. W. Chung, C. W. Shu, K. P. Chuang, T. H. Duh, M. H. Yang and Y. C. Tyan, Hydrogels: Properties and applications in biomedicine, *Molecules*, 2022, **27**(9), 2902, DOI: 10.3390/molecules27092902.

8 K. V. G. Sinad, R. C. Ebubechukwu and C. K. Chu, Recent advances in double network hydrogels based on naturally-derived polymers: Synthesis, properties, and biological applications, *J. Mater. Chem. B*, 2023, **11**(48), 11460–11482, DOI: 10.1039/D3TB00773A.

9 H. K. Pradeep, D. H. Patel, M. Laxmi, C. C. Pratiksha, B. Girish, G. M. P. Kumar, S. Abhay and H. M. M. Kumar, Pharmaceutical hydrogels: A comprehensive review, *RGUHS J. Pharm. Sci.*, 2024, **14**(2), 1–13, DOI: 10.26463/rjps.14_2_7.

10 S. Bashir, M. Hina, J. Iqbal, A. H. Rajpar, M. A. Mujtaba, N. A. Alghamdi, S. Wageh, K. Ramesh and S. Ramesh, Fundamental concepts of hydrogels: Synthesis, properties, and their applications, *Polymers*, 2020, **12**(11), 2702, DOI: 10.3390/polym12112702.

11 X. Sun, F. Yao and J. Li, Nanocomposite hydrogel-based strain and pressure sensors: A review, *J. Mater. Chem. A*, 2020, **8**(36), 18605–18623, DOI: 10.1039/D0TA06965E.

12 P. Yang, F. Zhu, Z. Zhang, Y. Cheng, Z. Wang and Y. Li, Stimuli-responsive polydopamine-based smart materials, *Chem. Soc. Rev.*, 2021, **50**(14), 8319–8343, DOI: 10.1039/D1CS00374G.

13 Z. Ahmad, S. Salman, S. A. Khan, A. Amin, Z. U. Rahman, Y. O. Al-Ghamdi, K. Akhtar, E. M. Bakhsh and S. B. Khan, Versatility of hydrogels: From synthetic strategies, classification, and properties to biomedical applications, *Gels*, 2022, **8**(3), 167, DOI: 10.3390/gels8030167.

14 B. Kaczmarek, K. Nadolna and A. Owczarek, The physical and chemical properties of hydrogels based on natural polymers ed. Y. Chen in *Hydrogels Based on Natural Polymers*, Elsevier, 2022, pp. 151–172, doi: DOI: 10.1016/B978-0-12-816421-1.00006-9.

15 R. Ahmad, O. S. Wolfbeis, Y. B. Hahn, H. N. Alshareef, L. Torsi and K. N. Salama, Deposition of nanomaterials: A crucial step in biosensor fabrication, *Mater. Today Commun.*, 2018, **17**, 289–321, DOI: 10.1016/j.mtcomm.2018.09.024.

16 J. W. Meisel and G. W. Gokel, A simplified direct lipid mixing lipoplex preparation: Comparison of liposomal-, dimethylsulfoxide-, and ethanol-based methods, *Sci. Rep.*, 2016, **6**(1), 27662, DOI: 10.1038/srep27662.

17 R. Bharti, S. Pal, N. Prasad, Y. Kumar, B. Joseph, H. Sharma and G. K. Sahu, A comprehensive review on hydrogel, *Acta Sci. Pharm. Sci.*, 2024, **8**(6), 64–75, DOI: 10.31080/ASPS.2024.08.1070.

18 S. Ahmad, M. Ahmad, K. Manzoor, R. Purwar and S. Ikram, A review on latest innovations in natural gums based hydrogels: Preparations & applications, *Int. J. Biol. Macromol.*, 2019, **136**, 870–890, DOI: 10.1016/j.ijbiomac.2019.06.113.

19 F. Naqash, F. A. Masoodi, S. A. Rather, S. M. Wani and A. Gani, Emerging concepts in the nutraceutical and functional properties of pectin—A review, *Carbohydr. Polym.*, 2020, **168**, 227–239, DOI: 10.1016/j.carbpol.2017.03.058.

20 S. J. Marathe, S. B. Jadhav, S. B. Bankar, K. K. Dubey and R. S. Singhal, Improvements in the extraction of bioactive compounds by enzymes, *Curr. Opin. Food Sci.*, 2019, **25**, 62–72, DOI: 10.1016/j.cofs.2019.02.009.

21 C. Nunes, L. Silva, A. P. Fernandes, R. P. F. Guiné, M. R. M. Domingues and M. A. Coimbra, Occurrence of cellobiose residues directly linked to galacturonic acid in pectic polysaccharides, *Carbohydr. Polym.*, 2012, **87**(1), 620–626, DOI: 10.1016/j.carbpol.2011.08.027.

22 S. Y. Chan, W. S. Choo, D. J. Young and X. J. Loh, Pectin as a rheology modifier: Origin, structure, commercial production and rheology, *Carbohydr. Polym.*, 2017, **161**, 118–139, DOI: 10.1016/j.carbpol.2016.12.033.

23 I. L. G. Lekhuleni, T. E. Kgatla, M. E. Mashau and A. I. O. Jideani, Physicochemical properties of South African prickly pear fruit and peel: Extraction and characterisation of pectin from the peel, *Open Agric.*, 2021, **6**(1), 178–191, DOI: 10.1515/opag-2021-0216.

24 F. V. Vityazev, M. I. Fedyuneva, V. V. Golovchenko, O. A. Patova, E. U. Ipatova, E. A. Durnev, E. A. Martinson and S. G. Litvinets, Pectin–silica gels as matrices for controlled drug release in gastrointestinal tract, *Carbohydr. Polym.*, 2017, **157**, 9–20, DOI: 10.1016/j.carbpol.2016.09.048.

25 R. Awasthi, G. T. Kulkarni, M. V. Ramana, T. J. A. Pinto, I. S. Kikuchi, D. D. M. Ghisleni, M. S. Braga, P. De Bank and K. Dua, Dual crosslinked pectin–alginate network as sustained release hydrophilic matrix for repaglinide, *Int. J. Biol. Macromol.*, 2017, **97**, 721–732, DOI: 10.1016/j.ijbiomac.2017.01.050.

26 L. Neufeld and H. Bianco-Peled, Pectin–chitosan physical hydrogels as potential drug delivery vehicles, *Int. J. Biol. Macromol.*, 2017, **101**, 852–861, DOI: 10.1016/j.ijbiomac.2017.03.167.

27 S. Thakur, J. Chaudhary, V. Kumar and V. K. Thakur, Progress in pectin based hydrogels for water purification: Trends and challenges, *J. Environ. Manage.*, 2019, **238**, 210–223, DOI: 10.1016/j.jenvman.2019.03.002.

28 J. Long, A. E. Etxeberria, A. V. Nand, C. R. Bunt, S. Ray and A. Seyfoddin, A 3D printed chitosan–pectin hydrogel wound dressing for lidocaine hydrochloride delivery, *Mater. Sci. Eng., C*, 2019, **104**, 109873, DOI: 10.1016/j.msec.2019.109873.

29 G. Wang, H. Li, X. Shao, S. Teng and Q. Wu, Design and development of pH-responsive levofloxacin-loaded metal–organic framework for the promising treatment of

pediatric abdominal wound repair, *Regener. Ther.*, 2024, **26**, 170–179, DOI: 10.1016/j.reth.2024.05.003.

30 Y. Zou, T. Wang, X. Lin, L. Yang and Y. Li, Regulation of the Light Absorption and Photothermal Performance of Melanin-Like Polymers, *Acc. Chem. Res.*, 2025, **58**(18), 2815–2829, DOI: 10.1021/acs.accounts.5c00346.

31 K. Elkhoury, M. Morsink, L. Sanchez-Gonzalez, C. Kahn, A. Tamayol and E. Arab-Tehrany, Biofabrication of natural hydrogels for cardiac, neural, and bone tissue engineering applications, *Bioact. Mater.*, 2021, **6**(11), 3904–3923, DOI: 10.1016/j.bioactmat.2021.03.040.

32 H. Chamkouri, A review of hydrogels, their properties and applications in medicine, *Am. J. Biomed. Sci. Res.*, 2021, **11**(6), 485–493, DOI: 10.34297/AJBSR.2021.11.001682.

33 S. S. Ferreira, C. P. Passos, P. Madureira, M. Vilanova and M. A. Coimbra, Structure–function relationships of immunostimulatory polysaccharides: A review, *Carbohydr. Polym.*, 2015, **132**, 378–396, DOI: 10.1016/j.carbpol.2015.05.079.

34 N. El Fihry, K. El Mabrouk, M. Eeckhout, H. A. Schols, Y. Filali-Zegzouti and H. Hajjaj, Physicochemical and functional characterization of pectin extracted from Moroccan citrus peels, *LWT*, 2022, **162**, 113508, DOI: 10.1016/j.lwt.2022.113508.

35 S. C. Teixeira, N. O. Gomes, T. V. Oliveira, P. Fortes-Da-Silva, N. F. Soares and P. A. Raymundo-Pereira, Review and perspectives of sustainable, biodegradable, eco-friendly and flexible electronic devices and (bio)sensors, *Biosens. Bioelectron.:X*, 2023, **14**, 100371, DOI: 10.1016/j.biosx.2023.100371.

36 A. Alam, Y. Zhang, H. C. Kuan, S. H. Lee and J. Ma, Polymer composite hydrogels containing carbon nanomaterials—Morphology and mechanical and functional performance, *Prog. Polym. Sci.*, 2018, **77**, 1–18, DOI: 10.1016/j.progpolymsci.2017.09.001.

37 S. Chungyampin, W. Charerntanom, P. Pakawanit, N. Paradee and S. Niamlang, Humidity-responsive actuators of synthesized graphene oxide/gelatin composite hydrogels: Effect of oxidation degree of graphene oxide, *Sens. Actuators, A*, 2024, **380**, 116032, DOI: 10.1016/j.sna.2024.116032.

38 R. T. Shafranek, S. C. Millik, P. T. Smith, C. U. Lee, A. J. Boydston and A. Nelson, Stimuli-responsive materials in additive manufacturing, *Prog. Polym. Sci.*, 2019, **93**, 36–67, DOI: 10.1016/j.progpolymsci.2019.03.002.

39 Z. Suhail, H. Shoukat, N. Sanbhal, N. Chowdhry, M. A. Bhutto, S. A. Soomro, A. Q. Ansari and R. H. Memon, Controlled drug release and antibacterial properties of levofloxacin-loaded silk/chitosan green composite for wound dressing, *Biomed. Mater. Dev.*, 2023, **1**(2), 796–804, DOI: 10.1007/s44174-022-00048-7.

40 A. Valizadeh, M. Shirzad, M. R. Pourmand, M. Farahmandfar, H. Sereshti and A. Amani, Levofloxacin nanoemulsion gel has a powerful healing effect on infected wound in streptozotocin-induced diabetic rats, *Drug Deliv. Transl. Res.*, 2021, **11**(1), 292–304, DOI: 10.1007/s13346-020-00794-5.

41 C. Cha, S. R. Shin, X. Gao, N. Annabi, M. R. Dokmeci, X. Tang and A. Khademhosseini, Controlling mechanical properties of cell-laden hydrogels by covalent incorporation of graphene oxide, *Small*, 2014, **10**(3), 514–523, DOI: 10.1002/smll.201302182.

42 E. Zhang, J. Yang and W. Liu, Cellulose-based hydrogels with controllable electrical and mechanical properties, *Z. Phys. Chem.*, 2018, **232**(9–11), 1707–1716, DOI: 10.1515/zpch-2018-1133.

43 C. Santillo, Y. Wang, G. G. Buonocore, G. Gentile, L. Verdolotti, S. Kaciulis and M. Lvorgna, Hybrid graphene oxide/cellulose nanofillers to enhance mechanical and barrier properties of chitosan-based composites, *Front. Chem.*, 2022, **10**, 926364, DOI: 10.3389/fchem.2022.926364.

44 N. I. Zaaba, K. L. Foo, U. Hashim, S. J. Tan, W. W. Liu and C. H. Voon, Synthesis of graphene oxide using modified Hummers method: Solvent influence, *Procedia Eng.*, 2017, **184**, 469–477, DOI: 10.1016/j.proeng.2017.04.118.

45 N. Batool, R. M. Sarfraz, A. Mahmood, U. Rehman, M. Zaman, S. Akbar, D. M. Almasri and H. A. Gad, Development and evaluation of cellulose derivative and pectin based swellable pH responsive hydrogel network for controlled delivery of cytarabine, *Gels*, 2023, **9**(1), 60, DOI: 10.3390/gels9010060.

46 A. Kharazmi, N. Faraji, R. Hussin, E. Saion, M. Yunus, W. M. M. Yunus and K. Behzad, Structural, optical, opto-thermal and thermal properties of ZnS–PVA nanofluids synthesized through a radiolytic approach, *Beilstein J. Nanotechnol.*, 2015, **6**, 529–536, DOI: 10.3762/bjnano.6.55.

47 V. C. Karade, A. Sharma, R. P. Dhavale, S. R. Shingte, P. S. Patil, J. H. Kim, D. R. T. Zahn, A. D. Chougale, G. Salvan and P. B. Patil, APTES monolayer coverage on self-assembled magnetic nanospheres for controlled release of anticancer drug Nintedanib, *Sci. Rep.*, 2021, **11**(1), 5674, DOI: 10.1038/s41598-021-84770-0.

48 D. Chen, X. Ma, J. Zhu, Y. Wang, S. Guo and J. Qin, Pectin based hydrogel with covalent coupled doxorubicin and limonin loading for lung tumor therapy, *Colloids Surf., B.*, 2024, **234**, 113670, DOI: 10.1016/j.colsurfb.2023.113670.

49 G. W. Oh, I. W. Choi, W. Park, C. Oh, S. J. Heo, D. H. Kang and W. K. Jung, Preparation and properties of physically cross-linked PVA/pectin hydrogels blended at different ratios for wound dressings, *J. Appl. Polym. Sci.*, 2022, **139**(9), e51696, DOI: 10.1002/app.51696.

50 T. Al Hagbani, B. Vishwa, A. S. Abu Lila, H. F. Alotaibi, E. S. Khafagy, A. Moin and D. V. Gowda, Pulmonary targeting of levofloxacin using microsphere-based dry powder inhalation, *Pharmaceutics*, 2022, **15**(5), 560, DOI: 10.3390/ph15050560.

51 L. Benassi, I. Alessandri and I. Vassalini, Assessing Green Methods for Pectin Extraction from Waste Orange Peels, *Molecules*, 2021, **26**, 1766, DOI: 10.3390/molecules26061766.

52 A. Zarinwall, T. Waniek, R. Saadat, U. Braun, H. Sturm and G. Garnweitner, Comprehensive Characterization of APTES Surface Modifications of Hydrous Boehmite Nanoparticles, *Langmuir*, 2021, **37**(1), 171–179, DOI: 10.1021/acs.langmuir.0c02682.

53 J. Nisar, M. Iqbal, A. Shah, M. S. Akhter, M. Sirajuddin, R. A. Khan, I. Uddin, L. A. Shah and M. S. Khan, Decomposition Kinetics of Levofloxacin: Drug-Excipient Interaction, *Z. Phys. Chem.*, 2020, **234**(1), 117–128, DOI: 10.1515/zpch-2018-1273.

54 P. Miao, J. Gao, X. Han, Y. Zhao and T. Chen, Adsorption of Levofloxacin onto Graphene Oxide/Chitosan Composite Aerogel Microspheres, *Gels*, 2024, **10**(1), 81, DOI: 10.3390/gels10010081.

55 M. A. U. R. Qureshi, N. Arshad and A. Rasool, Graphene Oxide Reinforced Biopolymeric (Chitosan) Hydrogels for Controlled Cephradine Release, *Int. J. Biol. Macromol.*, 2023, **242**, 124948, DOI: 10.1016/j.ijbiomac.2023.124948.

56 M. A. U. R. Qureshi, N. Arshad, A. Rasool, M. Rizwan and T. Rasheed, Guar Gum-Based Stimuli Responsive Hydrogels for Sustained Release of Diclofenac Sodium, *Int. J. Biol. Macromol.*, 2023, **250**, 126275, DOI: 10.1016/j.ijbiomac.2023.126275.

57 F. Souza Almeida, K. C. Guedes Silva, A. Matias Navarrete de Toledo and A. C. Kawazoe Sato, Modulating Porosity and Mechanical Properties of Pectin Hydrogels by Starch Addition, *J. Food Sci. Technol.*, 2021, **58**(1), 302–310, DOI: 10.1007/s13197-020-04543-x.

58 R. R. Vildanova, S. F. Petrova, S. V. Kolesov and V. V. Khutoryanskiy, Biodegradable Hydrogels Based on Chitosan and Pectin for Cisplatin Delivery, *Gels*, 2023, **9**(4), 342, DOI: 10.3390/gels9040342.

59 J. Li, C. Peng, A. Mao, M. Zhong and Z. Hu, An Overview of Microbial Enzymatic Approaches for Pectin Degradation, *Int. J. Biol. Macromol.*, 2024, **254**(Pt 1), 127804, DOI: 10.1016/j.ijbiomac.2023.127804.

60 A. S. Luis, J. Briggs, X. Zhang, B. Farnell, D. Ndeh, A. Labourel, A. Baslé, A. Cartmell, N. Terrapon, K. Stott, E. C. Lowe, R. McLean, K. Shearer, J. Schückel, I. Venditto, M. C. Ralet, B. Henrissat, E. C. Martens, S. C. Mosimann and H. J. Gilbert, Dietary Pectic Glycans Are Degraded by Coordinated Enzyme Pathways in Human Colonic Bacteroides, *Nat. Microbiol.*, 2018, **3**(2), 210–219, DOI: 10.1038/s41564-017-0079-1.

61 A. Herrmann, R. Haag and U. Schedler, Hydrogels and Their Role in Biosensing Applications, *Adv. Health Mater.*, 2021, **10**(11), 2100062, DOI: 10.1002/adhm.202100062.

62 B. Adhikari, A. Biswas and A. Banerjee, Graphene Oxide-Based Hydrogels to Make Metal Nanoparticle-Containing Reduced Graphene Oxide-Based Functional Hybrid Hydrogels, *ACS Appl. Mater. Interfaces*, 2012, **4**(10), 5472–5482, DOI: 10.1021/am301373n.

63 V. Ravikumar, I. Mijakovic and S. Pandit, Antimicrobial Activity of Graphene Oxide Contributes to Alteration of Key Stress-Related and Membrane Bound Proteins, *Int. J. Nanomed.*, 2022, **17**, 6707–6721, DOI: 10.2147/IJN.S387590.

64 N. Ajaz, I. Khalid, M. U. Minhas, K. Barkat, I. U. Khan, H. K. Syed, S. Asghar, R. Munir and F. Aslam, Pectin-Based Hydrogels with Adjustable Properties for Controlled Delivery of Nifedipine: Development and Optimization, *Polym. Bull.*, 2020, **77**(11), 6063–6083, DOI: 10.1007/s00289-019-03065-7.

65 L. Rueda-Gensini, J. A. Serna, J. Cifuentes, J. C. Cruz and C. Muñoz-Camargo, Graphene Oxide-Embedded Extracellular Matrix-Derived Hydrogel as a Multiresponsive Platform for 3D Bioprinting Applications, *Int. J. Bioprinting.*, 2021, **7**(3), 353, DOI: 10.18063/ijb.v7i3.353.

66 F. V. Lavrentev, V. V. Shilovskikh, V. S. Alabusheva, V. Yu. Yurova, A. A. Nikitina, S. A. Ulasevich and E. V. Skorb, Diffusion-Limited Processes in Hydrogels with Chosen Applications from Drug Delivery to Electronic Components, *Molecules*, 2023, **28**(15), 5931, DOI: 10.3390/molecules28155931.

67 D. U. Kapoor, R. Garg, M. Gaur, A. Pareek, B. G. Prajapati, G. R. Castro, S. Suttiruengwong and P. Sriamornsak, Pectin Hydrogels for Controlled Drug Release: Recent Developments and Future Prospects, *Saudi Pharm. J.*, 2024, **32**(4), 102002, DOI: 10.1016/j.jsps.2024.102002.

68 J. Wang, C. Zhao, S. Zhao, X. Lu, M. Ma and J. Zheng, Gelling Properties of Lysine-Amidated Citrus Pectins: The Key Role of pH in Both Amidation and Gelation, *Carbohydr. Polym.*, 2023, **317**, 121087, DOI: 10.1016/j.carbpol.2023.121087.

69 D. Gawkowska, J. Cybulska and A. Zdunek, Structure-Related Gelling of Pectins and Linking with Other Natural Compounds: A Review, *Polymers*, 2018, **10**(7), 762, DOI: 10.3390/polym10070762.

70 N. Mohamad Nor, S. Arivalakan, N. D. Zakaria, N. Nilamani, Z. Lockman and K. Abdul Razak, Self-Assembled Iron Oxide Nanoparticle-Modified APTES-ITO Electrode for Simultaneous Stripping Analysis of Cd(II) and Pb(II) Ions, *ACS Omega*, 2022, **7**(4), 3823–3833, DOI: 10.1021/acsomega.1c07158.

71 A. Rasool, S. Ata, A. Islam and R. U. Khan, Fabrication of Novel Carrageenan-Based Stimuli Responsive Injectable Hydrogels for Controlled Release of Cephradine, *RSC Adv.*, 2019, **9**(22), 12282–12290, DOI: 10.1039/C9RA02130B.

72 M. Rizwan, R. Yahya, A. Hassan, M. Yar, A. D. Azzahari, V. Selvanathan, F. Sonsudin and C. N. pH. Abouloula, Sensitive Hydrogels in Drug Delivery: Brief History, Properties, Swelling, and Release Mechanism, Material Selection and Applications, *Polymers*, 2017, **9**(4), 137, DOI: 10.3390/polym9040137.

73 N. H. Thang, T. B. Chien and D. X. Cuong, Polymer-Based Hydrogels Applied in Drug Delivery: An Overview, *Gels*, 2023, **9**(7), 523, DOI: 10.3390/gels9070523.

74 R. Wang, C. Cheng, H. Wang and D. Wang, Swollen Hydrogel Nanotechnology: Advanced Applications of the Rudimentary Swelling Properties of Hydrogels, *Mater. Chem. Phys.*, 2024, **3**(4), 357–375, DOI: 10.1016/j.chphma.2024.07.006.

75 G. Giusto, G. Beretta, C. Vercelli, E. Valle, S. Iussich, R. Borghi, P. Odetti, F. Monacelli, C. Tramuta, E. Grego, P. Nebbia, P. Robino, R. Odore and M. Gandini, Pectin-Honey Hydrogel: Characterization, Antimicrobial Activity and Biocompatibility, *Bio-Med. Mater. Eng.*, 2018, **29**(3), 347–356, DOI: 10.3233/BME-181730.

76 K. Olczak, W. Jakubowski and W. Szymański, Bactericidal Activity of Graphene Oxide Tests for Selected Microorganisms, *Materials*, 2023, **16**(11), 4199, DOI: 10.3390/ma16114199.

77 M. A. U. R. Qureshi, N. Arshad, A. Rasool, M. Rizwan, K. F. Fawy and T. Rasheed, pH-Responsive Chitosan Dendrimer Hydrogels Enabling Controlled Cefixime Release, *Eur. Polym. J.*, 2024, **219**, 113377, DOI: 10.1016/j.eurpolymj.2024.113377.

78 R. P. Gazzi, L. A. Frank, G. Onzi, A. R. Pohlmann and S. S. Guterres, New Pectin-Based Hydrogel Containing Imiquimod-Loaded Polymeric Nanocapsules for Melanoma Treatment, *Drug Deliv. Transl. Res.*, 2020, **10**(6), 1829–1840, DOI: 10.1007/s13346-020-00805-5.

79 H. Manzoor, N. Arshad, M. A. U. R. Qureshi and A. Javed, Hydroxyapatite-reinforced pectin hydrogel films PEC/PVA/APTES/HAp: doxycycline loading for sustained drug release and wound healing applications, *RSC Adv.*, 2025, **15**(37), 30026–30045, DOI: 10.1039/D5RA04341G.

80 M. A. U. R. Qureshi, N. Arshad, A. Rasool, N. K. Janjua, M. S. Butt, M. N. U. R. Qureshi and H. Ismail, Kappa-carrageenan and sodium alginate-based pH-responsive hydrogels for controlled release of methotrexate, *Royal. Soc. Open Sci.*, 2024, **11**(4), 231952, DOI: 10.1098/rsos.231952.

81 K. Aliyeva, A. Albayrak, E. Toktay, E. E. Yurdgulu and Y. Bayir, The Role of Pectin Hydrogel Systems Plus Iodine and Phyto Extract in Second-Degree Burn in Rats, *Eurasian J. Med.*, 2024, **56**(3), 170–177, DOI: 10.5152/eurasianjmed.2024.24550.

82 V. Gounden and M. Singh, Hydrogels and Wound Healing: Current and Future Prospects, *Gels*, 2024, **10**(1), 43, DOI: 10.3390/gels10010043.

83 Y. Yao, A. Zhang, C. Yuan, X. Chen and Y. Liu, Recent Trends on Burn Wound Care: Hydrogel Dressings and Scaffolds, *Biomater. Sci.*, 2021, **9**(13), 4523–4540, DOI: 10.1039/D1BM00411E.

84 B. Kocaaga, T. Inan, N. I. Yasar, C. E. Yalcin, F. A. Sungur, O. Kurkcuoglu, A. Demiroz, H. Komurcu, O. Kizilkilic, S. Y. Aydin, O. Aydin Ulgen, F. S. Güner and H. Arslan, Innovative Use of an Injectable, Self-Healing Drug-Loaded Pectin-Based Hydrogel for Micro- and Supermicro-Vascular Anastomoses, *Biomacromolecules*, 2024, **25**(7), 3959–3975, DOI: 10.1021/acs.biomac.4c00102.

85 C. Lu, Q. Sun, Z. Li, Y. Wei, J. Yu, S. Li, Y. S. Wang, K. Li, C. Tang, H. Cao, J. Chen, Q. Liu, X. Liang, S. Zhang, C. Xie and B. Tang, Injectable Glycyrrhizinate-Pectin Hydrogel Wound Dressing Based on Natural Ingredients, *Carbohydr. Polym.*, 2025, **359**, 123562, DOI: 10.1016/j.carbpol.2025.123562.

86 G. Divyashri, R. V. Badhe, B. Sadanandan, V. Vijayalakshmi, M. Kumari, P. Ashrit and A. V. Raghu, Applications of Hydrogel-Based Delivery Systems in Wound Care and Treatment: An Up-to-Date Review, *Polym. Adv. Technol.*, 2022, **33**(7), 2025–2043, DOI: 10.1002/pat.5661.

87 W. Zhang, L. Liu, H. Cheng, J. Zhu, X. Li, S. Ye and X. Li, Hydrogel-Based Dressings Designed to Facilitate Wound Healing, *Mater. Adv.*, 2024, **5**(4), 1364–1394, DOI: 10.1039/D3MA00682D.

88 D. Solanki, P. Vinchhi and M. M. Patel, Design Considerations, Formulation Approaches, and Strategic Advances of Hydrogel Dressings for Chronic Wound Management, *ACS Omega*, 2023, **8**(9), 8172–8189, DOI: 10.1021/acsomega.2c06806.

89 Y. Hu, B. Yu, Y. Jia, M. Lei, Z. Li, H. Liu, H. Huang, F. Xu, J. Li and Z. Wei, Hyaluronate- and Gelatin-Based Hydrogels Encapsulating Doxycycline as a Wound Dressing for Burn Injury Therapy, *Acta Biomater.*, 2023, **164**, 151–158, DOI: 10.1016/j.actbio.2023.04.021.

90 M. Rezvanian, N. Ahmad, M. C. I. Mohd Amin and S. F. Ng, Optimization, Characterization, and In Vitro Assessment of Alginate-Pectin Ionic Cross-Linked Hydrogel Film for Wound Dressing Applications, *Int. J. Biol. Macromol.*, 2017, **97**, 131–140, DOI: 10.1016/j.ijbiomac.2016.12.079.

91 K. Z. M. Valle, R. A. Saucedo Acuña, J. V. Ríos Arana, N. Lobo, C. Rodriguez, J. C. Cuevas-Gonzalez and K. L. Tovar-Carrillo, Natural Film Based on Pectin and Allantoin for Wound Healing: Obtaining, Characterization, and Rat Model, *Biomed. Res. Int.*, 2020, **2020**, 6897497, DOI: 10.1155/2020/6897497.

92 N. Arshad, A. A. Chaudhary, S. Saleem, M. Akram and M. A. U. R. Qureshi, Surface Modification of Surgical Suture by Chitosan-Based Biocompatible Hybrid Coatings: In Vitro Anti-Corrosion, Antibacterial, and In Vivo Wound Healing Studies, *Int. J. Biol. Macromol.*, 2024, **481**(4), 136571, DOI: 10.1016/j.ijbiomac.2024.136571.

93 Y. Wang, S. Liu and W. Yu, Functionalized Graphene Oxide-Reinforced Chitosan Hydrogel as Biomimetic Dressing for Wound Healing, *Macromol. Biosci.*, 2021, **21**(4), 2000432, DOI: 10.1002/mabi.202000432.

94 Q. Yu, C. Shen, X. Wang, Z. Wang, L. Liu and J. Zhang, Graphene Oxide/Gelatin Nanofibrous Scaffolds Loaded with N-Acetyl Cysteine for Promoting Wound Healing, *Int. J. Nanomed.*, 2023, **18**, 563–578, DOI: 10.2147/IJN.S392782.